EFFECTS OF THE MECHANICAL MICROENVIRONMENT ON EARLY AVIAN MORPHOGENESIS

A Dissertation
Presented to
The Academic Faculty

by

Julia Ann Henkels

In Partial Fulfillment
of the Requirements for the Degree
Doctor of Philosophy in Bioengineering in the
George W. Woodruff School of Mechanical Engineering

Georgia Institute of Technology
May 2013

EFFECTS OF THE MECHANICAL MICROENVIRONMENT ON EARLY AVIAN MORPHOGENESIS

Approved by:

Dr. Evan Zamir, Advisor
George W. Woodruff School of
Mechanical Engineering
Georgia Institute of Technology

Dr. Andrés García, Co-Advisor
George W. Woodruff School of
Mechanical Engineering
Georgia Institute of Technology

Dr. Todd Sulchek
George W. Woodruff School of
Mechanical Engineering
Georgia Institute of Technology

Dr. Thomas Barker
Wallace H. Coulter Department of
Biomedical Engineering
Georgia Institute of Technology

Dr. Andrew Kowalczyk
Departments of Cell Biology and
Dermatology
Emory University

Date Approved: 12 May 2013

To my parents, Robert and Mary,

and the indispensables: Kathy, Jane, Joe, Peter, and Anna

ACKNOWLEDGEMENTS

I am humbled at the number of people who have supported me in this work.

I must begin by thanking my advisor, Dr. Evan Zamir. When I began emailing with Evan in the Fall of 2007, I was struck by his enthusiasm for his work, and it was contagious. Evan has an impeccable knowledge of the literature and endless new ideas. Along with his intellect, he shared with the lab his love of sushi, the ways of Californians, and most products made by Apple, of which he is a connoisseur. I'll miss our lab lunches all around the city and scheming up crazy ideas during our lab meetings (research-related and not). I am very fortunate to have him for a mentor, and if I had it to do over, I'd rejoin his lab in a heartbeat. It has been a privilege working with him, and I can't thank him enough for everything he has taught me and for always pushing me to do better.

I owe a debt of gratitude to Dr. Andrés García, who was the reason I considered Tech in the first place after his dynamic presentation on cell mechanics at Notre Dame. He introduced me to my advisor, helped me assimilate into Georgia Tech culture, and answered all my questions after his Advanced Biomaterials class during my first semester (such as, "what is a protein?") As the Bioengineering Program Chair, he supported my efforts to "brand" the BioE program, he introduced me to chicharrón, and he was always ready with "The García Pep-talk," which, I found out later from his students, is patented. His support and encouragement have been particularly indispensable in my final year.

Dr. Todd Sulchek has been an invaluable collaborator in my research, and I've taken advantage of his open-door policy more than once to discuss a new AFM challenge. I am grateful for his creative problem solving, kindly allowing me to use his

AFM in its not-so-easy-bake oven/alien life pod/what you will, and his down-to-earth approachability, even when he is swarmed with undergraduate students.

Dr. Thomas Barker kindly allowed me to be privy to the top-secret successful protocols of the Barker lab, such as PA gel manufacturing, Western blotting, and crosslinking fibronectin. He has been particularly helpful with the ECM details of my project, and I am grateful for his contributions.

Dr. Andrew Kowalczyk contributed to my project in particular by providing perspective on the importance of hypothesis-driven research and his expertise in cell biology. He is a good and thoughtful listener and helped me keep in mind the "big picture" of my research.

I would like to thank the members of the Zamir Lab for a memorable run. We may have had differing opinions on "Doctor Who," and different levels of comic book knowledge, but I've enjoyed working with each of them. Our legendary Carver's lunches were worth the subsequent food coma. Jaeho Oh, a former Korean soldier, has no known weaknesses. His mercy prevented him from sneaking up on me while I was working in the hood, though it would have been all too easy. He is hands-down the best maker of cheesecake and Korean barbecue, and he always returns from trips abroad bearing gifts. He made the lab a fun place to work − I've never seen him in a bad mood − and I will miss having him around. Drew Owen was a major factor in my premature decision to attend DragonCon in a group costume—so far outside of my comfort zone, I still am not sure how I agreed to it. Drew is also a cigar connoisseur, and I'm grateful to him for celebrating my successful proposal with a couple cigars at Gordon Biersch. Most of all, Drew introduced me to roasted garlic, which is the mark of a true friend. Matt Futterman's carefree nature invited us all not to take ourselves too seriously, and he kindly provided many brownies, Oreo balls, and other confections to the lab, which were always welcome. John Glissen was the créme de la créme of undergrads at Tech and now continues to live the dream in grad school. He

knows lots of interesting facts - from dog breeds to optic bandpass filters - that make boring incubation times fly by, and he always has a smile and a good attitude.

Though it is not a well-known fact, I am the sole honorary member of the García Lab. Despite Andrés's insistence that the lab is a dictatorship and Dr. Tim Petrie's insistence that he had several votes due to seniority, I was voted into the lab by a majority vote in the Spring of 2008. This is an honor that I do not take lightly. Within the García Lab, I must begin by thanking Dr. David Dumbauld, who was my first friend in Atlanta. With no senior lab members to show me the ropes, Dave let me tag along and learn how to amplify plasmids with Qiagen Kits and smelly bacteria and never grew tired of all my questions. The kickball games with after-parties hosted by him and his wife Dr. Kelly Erby (her skills − from academics and writing to cooking to style − would take this entire volume to document) remain treasured memories of my time at Tech. And he still puts up with my requests for his advice and perspectives. Kelly and Dave's adopted son, Brent Uhrig a.k.a. Teen Wolf is always up for a laugh or a chat about careers, and will soon be a titan of industry like his [adopted] father. Dr. Sean Coyer, Dave's partner in crime and another first-week friend at Tech, was always ready to cheer me up, help with a question, or create a new nickname for me. His and his wife Shetal's outings in East Atlanta were always a welcome break from the lab and a good time.

Dr. Abbey Wojtowictz first introduced me to the Atlanta salsa scene, for which I am forever grateful. For a long time, we only talked about salsa dancing and dancing shoes, but it turns out she is a brilliant researcher in addition to being an exceptional dancer. I don't think she'll ever know how much her friendship and mentoring meant to me especially during those first years at Tech and at every step of my graduate career since. I look forward to many years of friendship with her and another brilliant researcher and talented salsero, Dr. Joe Charest. The wedding in Puerto Rico was by far one of my happiest memories of graduate school.

Dr. Ed Phelps, mountain climber and renaissance man, is one of the smartest people I know, yet he is also one of the most humble and kind. He will stop to help you on his busiest day. Nduka Enemchukwu is as genuine of an individual as I have ever met. Dr. Rachel Whitmire provided admirable leadership in the Bioengineering Graduate Student Advisory Committee (BGSAC) before handing me the reigns, and I'm grateful for her example and the opportunity. Rachel also introduced me to editing for AJE, and taught me that even with the toughest of projects, you can still find a way to the other side. Dr. Asha Shekaran is yet another person in IBB who seems too cool and personable to be such a research nerd. She is calm under pressure and always has a huge smile, a quirky t-shirt, or a funny story to brighten your day. I am grateful to Dr. Ankur Singh, who helped me immensely utilizing Dave and Ted's vinculin-staining protocol and his previous fibronectin-staining protocol. He was never too busy to give encouragement and seasoned advice on publishing. Ted Lee is the perfect combination of smart, realistic, and easy-going. Stacie Gutowski is a crafty one—she taught me how to make a butterfly ball, and among her many talents makes ornately-decorated and delicious baking creations. Kellie Templeman has been very kind to me from my first weeks at Tech, looking up item numbers or protocols without complaint. If she ever left, I believe the García Lab (and perhaps IBB) would collapse. Chi-Chi Esimai, Apoorva Kalasuramath, Dr. Susan Lehman, and Dr. Imen Hannachi all embody the hard-working and personable character of the García lab.

I cannot express enough thanks to The Mom Squad, a triune life-force team who took care of me when I had the H1N1 virus. They got me to an IV and medicine, and without them I would still be in a pile on the floor of my apartment. Dr. Andrea Para, my Polish sister, is the kind of friend who will drop everything and bend over backwards to help a friend at a moment's notice. We never decided who to blame, but we trained for and completed a couple marathons together and lived to tell about it.

As the shirts say, "26.2 miles: What could possibly go wrong??" The adventures were many. Oh, Andrea, thank you for not leaving me by the side of the road somewhere and sticking with me through the rain, snow, hail, and injuries. I was fortunate to have Dr. Laura Hansen sit near me in the office, and we went through all the ups and downs of research life together and still made time for birthday treats. Laura is an extremely talented scientist, but always makes it look easy. Her gourmet cooking is something to write home about. Tamera Scholz, AoD, Master of Most Things including but by no means limited to lemon pie, sewing dresses, and Mechanical Engineering, and I bonded immediately over a mutual love of dancing, especially salsa dancing. I will never forget our outings with Scarlett and the summer early in graduate school when we regularly presided over our favorite salsa venue.

I would like to thank all the members, past and present, of Wing 2A for making Tech one of the most interesting and at times hilarious places to work. I have enjoyed getting to know many of the Gleason Lab members. Dr. William Wan made graduate school seem like fun (maybe because he was previously a kindergarten teacher). He also shared his expert knowledge and advocacy of recycling and composting with rest of the wing. Julia Raykin has been kind enough to share her expert knowledge of Matlab and is always ready to help others with research. She has a personal strength that I admire. Prem Midha has talents enough for several careers. I would challenge any other duo in IBB to best our guitar sing-a-longs in lab. You just never know when you'll need live guitar music in lab—it really adds something to the atmosphere. I am also grateful to Prem for sharing his mastery of photoshop. Dr. Mike Zaucha and Dan Howell welcomed me into our cubicle section and kept me entertained with (sometimes daily) rearrangements of my desk. Dr. Roy Wang is a talented researcher but was never too busy to participate in philosophical discussions on any number of topics with his fellow cubicle-mates. Roy, Prem, and Seth Gazes sometimes mistook our wing for a locker room, but things were never dull with them around. Alex Caulk

is a real Southern gent who somehow managed to travel to Ethiopia, propose his thesis, and get married seemingly all at once. Kelly Straub planned a number of memorable outings and always kept her sense of humor in trials of research.

The Yoganathan Lab made their presence known with conversations across opposite ends of the wing. I will miss life chats with Dr. Choon Hwai Yap, JP Rabbah (who pretends not to care but does, sorry for blowing your cover, JP), Andrew Siefert (here's to the Peachtree Road Race!), Dr. Shiva Arjunon, Maria Restrepo, and Swetha Rathan. Dr. Chris Haggerty, Dr. Erin Spinner, and myself shared some memorable conference travels. Erin and I are forever bound by our adventures touring Asia after the World Congress of Biomechanics in Singapore. Erin not only gave me a running tour of Singapore and put up with my inability to sit still and lay on a beach, she also encouraged me to try exotic foods (too bad rain chased away the fried grasshopper carts in Cambodia!) and let me drag her out dancing in Thailand, an experience neither of us will soon forget. Professionally, Erin has a positive attitude, industriousness, and tenacity that I admire and try to emulate. I look forward to visits to the West Coast in the future to see her and dashing fiancé, Dr. Andrés Bratt-Leal.

I have enjoyed getting to know the members of the Ku lab of past and present and in particular, thanks are due to Marmar Merabadi for sharing her expert knowledge of LaTeX.

Thank you to the Forest Lab for their accommodating space sharing in these last months of my Ph.D. Mel(issa) Li, my partner in the race to the end and so much more than a "futurist," has gracefully and admirably navigated many challenges on the road to the finish line. She shares my love of coffee (it's a great source of antioxidants!) and a favorite quote is, "What? You people need more than coffee and research to live off of? Weaklings!" Burning Man Chris Phaneuf put all other IBB moustaches to shame and is an expert Frisbee player, as I found out at the memorable BGSAC Frisbee Golf Tournament. Dr. Suhasa Kodandaramaiah made IBB history by being

wheeled in post-defense in a wagon-cage contraption pulled by Dr. Craig Forest. I have (for unworthiness) declined the offer for the same honor. It's all you, Mel.

I thank the Barker Lab, including Dr. Ashley Carson Brown, Dr. Allyson Soon, Lizhi Cao, Vince Fiore, and Alison Douglas for sharing their space with me and answering multivarious protocol questions. Ashley has been an invaluable mentor in many ways. Not only did she teach me how to make polyacrylamide gels and share her Western blotting prowess, she passed along innumerable tips and stories about running and training for marathons, assorted running gear, and eating "gu." Chris Brown, a fellow Notre Dame fan, was always a gracious host at the Christmas parties and cookie parties. The Browns have run more miles than anyone I know, and I look forward to going out to brunch again after the next race!

Thanks to the Sulchek Lab for sharing their AFM with me and to Wenwei Xu, who beaded several cantilevers and kindly allowed me to use his own modified Igor software for time-saving force curve analysis.

Thank you to the entire BGSAC committee with whom I served. Patricia Pacheco, a salsera queen, is as much fun off the dance floor as on. No matter what is going on with life and research, Patch always has a smile. She dominated BGSAC Thanksgiving down to the personalized Thanksgiving greeting cards and makes a killer chocoflan. Ashley Allen, to whom I passed on the reigns of BGSAC, is a master of witty mass correspondence. I swear the BioEs didn't mind the spam when it was so clever. She's one of the few people I know who can pull off retina-burning pink running shoes.

Thank you also to the Woodruff School Graduate Women and my fellow officers, who were a great support and were always a good time from coffee breaks and lunches to Trees Atlanta volunteering and, Andrea, our pet project of TechTalks.

There are a number of friends, I'm happy to say, with whom I've spent no time whatsoever in the lab, but without whom my time at Tech would be incomplete

without girls nights, crafting nights, and dancing: Song Seto, Katie Pitz, Dr. Roxanne Moore (The Cake Engineer!), Dr. Casey Ankeny, Dr. Nnenna Finn (and Trevor!), Heidi Khalil, and Dr. Lindsey Goodman.

I would like to thank the whole staff of IBB who works to make everything we do possible. Particular thanks to Allen Echols, biker and baker extraordinaire (your hobby should be harder than your job to make your job feel better, right?) Thank you to Chris Ruffin for helping me with BGSAC organizing details and keeping track of all the BioE students. Thank you to Janice Russell and Sandra Powell for keeping track of me on the NIH fellowship, and to James Goddard and Floyd Wood for projector rentals and their behind-the-scenes work to keep IBB running smoothly.

A highlight of my experience at Tech was the Graduate Leadership Program. Thank you to Dr. Ravi Bellamkonda, Dr. Terry Blum, Kathleen Kurre, Dr. Johnna Temenoff, Dr. Robert Thomas, and Dr. Wendy Newstetter for giving of their time to our 2010-11 class.

I am grateful to the Georgia Tech Catholic Center community for their friendship and fellowship. Particular thanks to Fr. Tim Hepburn and Fr. Kevin Peek for giving tirelessly of their time and energy to the students at Tech. In addition, thank you to Drs. David and Michelle Ediger for single-handedly creating a graduate student community and convincing me to help organize and emcee a retreat for the Archdiocese of Atlanta Young Adult Ministry.

Special thanks to the Doroski family, who has become my family and who is now stuck with me forever as a godmother.

My time at Tech would be incomplete without the Atlanta Salsa and Swing Dancing scenes. Thank you to my instructors at Down South Swing and to Joby Brava and my performance team, Joby Brava Ladies. Dancing was always a healthy mental break from the lab when I could find the time. Thank you also to the Chattahoochee Road Runners for providing me with pre-mapped routes and Gatorade stops while

mentally working out research challenges on the pavement.

Thank you to the extended ND/HSP community and the Mosconas, Curtins, Flores, and Slonkoskys. I wish I could have more time here with them.

I am grateful to the Haigs and McGibbons for letting me spend time with their beautiful children and have some vicarious family life far away from family.

Thanks to my ND engineers for their support and encouragement and for putting up with my missing weekend trips and, yes, even Notre Dame football games to tend to the embryos.

G-JAM is the best thing that happened to me in the ATL, and I can never thank them enough.

Thank you to my Frassati Housemates for being themselves. Life without them would be second rate.

Thank you to my wonderful extended family, the Henkels, Chips, Halls, and Slonkoskys. I love you guys, and our parties are better than anyone else's.

My parents, Robert and Mary, and my siblings, Kathy, Jane, Joe, Peter, and Anna are, and have always been, an incredible support to me. They always believe in me more than I do myself, and I would be lost without them.

My greatest thanks goes to my Beloved.

Contents

List of Figures

SUMMARY

The objective of this work is to investigate the elastic modulus of gastrula-stage avian embryos and the effect of substrate stiffness on presumptive precardiac cell fate. Our overall hypothesis is that the mechanical microenvironment, specifically, tissue modulus and substrate stiffness, influences gastrulation and cardiac induction.

Large-scale morphogenetic movements during early embryo development are driven by complex changes in biochemical and biophysical factors. Current models for amniote primitive streak morphogenesis and gastrulation take into account numerous genetic pathways but largely ignore the role of mechanical forces. Here, we used atomic force microscopy (AFM) to obtain for the first time precise biomechanical properties of the early avian embryo. Our data reveal that the primitive streak is significantly stiffer than neighboring regions of the epiblast, and that it is stiffer than the pre-primitive streak epiblast. To test our hypothesis that these changes in mechanical properties are due to a localized increase of actomyosin contractility, we inhibited actomyosin contractility via the Rho kinase (ROCK) pathway using the small-molecule inhibitor Y-27632. Our results using several different assays show the following: 1) primitive streak formation was blocked; 2) the time-dependent increase in primitive streak stiffness was abolished; and 3) convergence of epiblast cells to the midline was inhibited. Taken together, our data suggest that actomyosin contractility is necessary for primitive streak morphogenesis, and specifically, ROCK plays a critical role. To better understand the underlying mechanisms of this fundamental process, future models should account for the findings presented in this study.

As presumptive cardiac cells traverse the course of differentiation into cardiac myocytes during cardiogenesis, the sequence, magnitude, and spatiotemporal map of

biomechanical and biochemical signals has not been fully explored. There have been many studies detailing the induction of cardiogenesis on a variety of substrates and ECM proteins, but none have completed a rigorous study of the effects of substrate stiffness on the induction of precardiac cells prior to the onset of cardiac gene expression (smooth muscle alpha actin [SMAA] at stage 5.) We investigate the effects of the mechanical environment on precardiac cell behaviors in an in vitro setting to elucidate the effect of substrate stiffness and inducing factors on precardiac tissue and the potential connection between them. The cells in the anterior portion of the primitive streak are fated to form the heart, and we show differing levels of SMAA expression on substrates of differing moduli, which suggests that substrate stiffness may play a role in cardiac differentiation. We cannot determine the physical mechanisms during morphogenesis without understanding the response of precardiac cells to changes in their mechanical environment.

Chapter I

SPECIFIC AIMS

Before the explosion of genetics research in the last century, embryonic development was largely studied from a mechanical perspective. Paired with genetic advances in understanding developmental signaling pathways and induction mechanisms, an important goal for understanding morphogenesis is to discover how the genome codes for changes in the mechanical movements of the embryonic cells.

The first feature of the amniote (reptiles, birds, mammals) embryo is the primitive streak (PS), which is formed during the critical developmental process of gastrulation. During gastrulation, cells converge to the rostral-caudal midline of the embryo and then ingress through the PS to form the three germ layers: endoderm, mesoderm, and ectoderm. There have been several molecular studies on the signaling pathways necessary for PS formation, but there are still active discussions and investigations of the underlying biophysical mechanisms at play. [15] [17] [16] [110] [118] Actomyosin-driven apical constriction has generally been accepted as one of the driving forces of gastrulation in anamiotes (fish, amphibians) [57] [50] [41] and lower organisms such as drosophila, [20] [65] sea urchins, [22] [23] [51] and cnidarians (jelly-fish, sea anemone). [104] [64] However, the prevailing wisdom in the field of avian primitive streak formation does not account for biophysical mechanisms and instead implicates chemotaxis [15] [18] [87] [109] and cell-cell intercalation. [110] We have previously shown that cells move in concert with the basal lamina, [118] suggesting that cells do not crawl over the basal lamina in response to a chemotactic gradient. It is understood in the field of mechanics that a stressed body has an increased apparent stiffness over its unstressed state. [117] This phenomenon has been exploited in previous cell

mechanics studies in which actomyosin contractility results in an increased cellular tension. [5] [80] [111] In this study, we present the mechanical properties of pre-and post-gastrula avian embryos, which implicate actomyosin contractility as a driving force of avian PS formation. Specifically, our hypothesis is that each "wave" of cells that progresses through the primitive streak constricts and then ingresses, and the subsequent wave of cells constricts and ingresses. Each individual cell constriction at the primitive streak contributes to the overall large-scale tissue movement of the epiblast toward the primitive streak.

The overall objective of this dissertation is 1) to measure the tissue modulus of gastrula-age embryos and the role of actomyosin contractility in gastrulation and 2) to determine if substrate stiffness has an effect on cardiac specification in precardiac embryo explants. Our overarching hypothesis is that 1) actomyosin contractility drives a stiffening of the primitive streak and cell convergence to the primitive streak and that 2) an increase in substrate stiffness will promote cardiac induction, as indicated by selected markers.

Specific Aim 1. Measure spatial and temporal changes in the tissue stiffness of pre- and post-gastrula amniote embryos. Use inhibitors to determine if changes in tissue stiffness are due to a localized increase of actomyosin contractility the primitive streak. *Our hypothesis is that increased actomyosin contractility along the primitive streak during gastrulation is indicated by an increase in tissue stiffness in the primitive streak.*

Before PS formation, cardiac progenitor cells reside in the posterior epiblast in Kollers Sickle [108]. They move anteriorly during PS formation and ingress through the anterior region of the PS during early gastrulation. Once in the mesoderm, cardiac precursor cells move anterolaterally, and at Hamburger Hamilton (HH) [40] stage 5 they begin to express the first cardiac-specific gene, smooth muscle alpha actin (SMAA) in the heart forming regions (HFR). SMAA expression marks the

onset of cardiac cell differentiation [85], and it is the major actin isoform in vascular tissue. [98] [19] The HFRs epithelialize, merge, and fuse along the ventral midline; folding occurs to create the primitive heart tube and beating begins. It was recently shown that there is an optimal substrate stiffness the contraction of differentiated embryonic cardiomyocytes harvested from developing avian embryos [31] and cardiac cells from formed embryonic hearts continue to show increased heart markers on increased substrate stiffnesses. [115] Many in vitro studies have been conducted to elucidate early developmental cardiac induction on a variety of surfaces, [68] [67] [55] [114] [30] [97] [99] [6] [91] [90] [37] yet no rigorous study has been completed to specify the role of substrate stiffness in pre-heart tube cardiac development. HH 3 marks the final stage prior to cardiac gene expression, and the HH 3 PS provides a source of undifferentiated potential cardiac cells with which to study the relationship between substrate stiffness, cell contractility, and heart induction. We aim to induce the expression of a cardiac differentiation marker, SMAA, within these cell populations to elucidate the effects of the substrate stiffness on the specification of developing heart tissue.

Specific Aim 2. Investigate the potential effects of substrate stiffness on the differentiation of presumptive precardiac cells. Quantify levels of SMAA expression in HH 3 anterior PS explant cultures in response to changes in substrate stiffness to elucidate the effect of substrate stiffness on cardiac specification. *Our hypothesis is that mechanical cues, specifically substrate stiffness, play a role in precardiac cell differentiation. Increased substrate stiffness leads to increased cardiac differentiation indicated by an increase in SMAA expression.*

The outcomes of this dissertation are as follows:

- There is no difference in tissue stiffness within the anterior, posterior, central, and lateral regions of the pre-gastrula embryo.
- In the post-gastrula embryo, the anterior and posterior primitive streak regions

are stiffer than the rest of the embryo.

- The anterior and posterior primitive streak in the post-gastrula embryo are more stiff than the pre-gastrula embryo.

- The post-gastrula embryo regions external to the primitive streak are softer than the pre-gastrula embryo.

These findings are significant because no such tissue stiffness mapping has previously been conducted on pre-somite avian embryos. The uniformity of stiffness in the pre-gastrula embryo (as well as cutting experiments previously conducted in our lab) suggests that the pre-gastrula embryo has no mechanical polarity at this stage, and the "forces that shape the embryo" [106] on the tissue-level scale are at a pause. Conversely, the increased stiffness in the primitive streak and decreased stiffness in the tissue surrounding the streak suggest that the tissue is no longer "at rest" but that the symphony of biophysical cues and operations - in concert with genetic and biochemical ones - is underway.

These results were surprising because although tissue stiffening has long been discussed as a developmental mechanism, tissue softening has enjoyed no such popularity. We hope that tissue softening, as well as tissue stiffening, will be considered as possible mechanisms in the future. It may be that both are used simultaneously ease tensile stress in regions adjacent to contracting tissue.

- When actomyosin contractility inhibitor Y-27632 was added to the embryos, the primitive streak did not show an increase in stiffness relative to regions outside the primitive streak and relative to pre-gastrula embryos.

This finding shows that actomyosin contractility is necessary for the increased stiffness at the primitive streak and supports our hypothesis that actomyosin contracility at the primitive streak "pulls" the cells in the epiblast toward the primitive streak during gastrulation.

- Time-lapse microscopy showed that when actomyosin contractility inhibitor Y-27632 was added to the embryos, the velocity of cell convergence to the primitive streak was slowed to half of the control velocity.

This finding further suggests that actomyosin contractility at the primitive streak − as indicated by an increase in tissue stiffness − is necessary for cell convergence to the primitive streak. This result is significant because current models of avian gastrulation do not include mechanical input, such as the forces generated by actomyosin contraction.

- Precardiac cells from the anterior primitive streak express higher levels of SMAA, the first cardiac marker, on "stiff" (70 kPa) substrates compared to "soft" (250 Pa) substrates.

Though previous studies have explanted precardiac cells from the primitive streak to examine the effects of biochemical factors, the majority of these have been conducted on glass as opposed to a deformable substrate. Differentiated 3-day-old cardiomyocytes have been grown on deformable substrates, but no studies have been completed to examine the effect of substrate stiffness on gastrula-stage cardiac precursors. Further, this study has the advantage of using the precise group of cells that would normally form the heart in vivo as opposed to an undifferentiated cell line.

- Posterior primitive streak cells express higher levels of E-cadherin on "soft" (250 Pa) substrates compared to "stiff" (70 kPa) substrates.

This finding is significant because although the posterior primitive streak is not fated to form the heart, it appears that this cell type at this stage is sensitive to substrate stiffness. The posterior primitive streak's sensitivity to substrate stiffness may effect the fate of these cells in vivo, including extraembryonic mesoderm and blood islands.

- Embryonic cardiomyocytes show no difference in SMAA and E-cadherin staining on "soft" (250 Pa) and "stiff" (70 kPa) substrates.

Whereas anterior and posterior primitive streak cells show differences in SMAA and E-cadherin staining on "soft" (250 Pa) and "stiff" (70 kPa) substrates, cardiomyocytes do not. This finding suggests that cardiomyocytes from 3-day-old embryos may be past a certain point of substrate-stiffness-dependent differentiation that occurs after stage HH 3, and that primitive streak cells from HH3 embryos have not passed this potential point of differentiation.

Chapter II

BACKGROUND

2.1 Overview

A cell's response to its microenvironment is influenced by interactions between the cell and 1) neighboring cells, 2) extracellular matrix (ECM) and fluid, and 3) soluble factors. Cells act as mechanical and chemical sensors as they adapt and respond to their environment, manifested in morphological changes, cytoskeletal remodeling, migration, differentiation, proliferation, and regulation of cell processes. From the formation of the zygote, numerous tissue migrations and foldings occur during each stage of development. How cells in the embryo generate and respond to forces is not fully known. The cell-cell and cell-matrix adhesions in this epithelial sheet likely serve as the footholds for generation of cytoskeletal (actomyosin) forces that ultimately shape the overall coordination of gastrulation and heart development. Neither the mechanical conditions necessary for this cell behavior, nor the contributions made by ECM adhesion and stiffness are currently known, and it is not possible to control these factors in vivo. In vitro experiments allow a controlled environment for further study the influence of the microenvironment on cell behaviors. Embryonic explantation studies have been used extensively to tease out regional cardiac induction signaling, but rigorous studies modulating the stiffness of the substrate for this stage of heart development have not been completed. An understanding of the native precardiac mechanical conditions would enable researchers to characterize these vital stages of development and identify contributions of biomechanical and biochemical signals essential for heart formation. We artificially vary the substrate compliance in

this study to determine if it might play a role in the developing embryo. By studying the mechanics in an external in vitro setting, we can isolate specific variables such as substrate stiffness and inducing factors and identify the potential relationship between them.

2.2 Gastrulation: The Mechanical Environment

Gastrulation, the formation of three germ layers in early morphologic development (Figure 1), occurs when epithelial cells in the epiblast undergo epithelial to mesenchymal transition (EMT), delaminate from the basement membrane (the thin ECM layer beneath the epiblast), and ingress through the primitive streak to form the mesoderm, the middle mesenchymal cell germ layer in the embryo, and the endoderm, the germ layer at the base of the embryo. While the mechanical environment within the HH 3 embryo has not been determined, cutting experiments [102] [101] at this stage result in an opening angle which indicates that there is tension and residual stress in the embryo, and it has been shown that tensile stresses promote migration in epithelial sheets. [103]

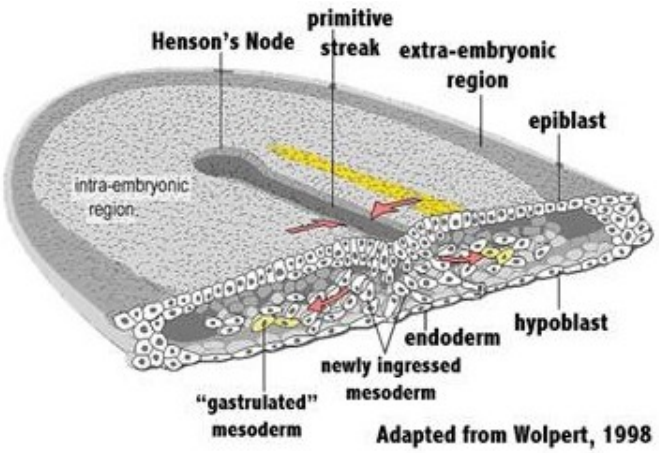

Figure 1: Avian Gastrulation

At this stage (HH 3), the primitive streak has formed and cardiac progenitor cells ingress through the anterior region of the streak.

EMT produces not only a change in cell attachment, but also a change in individual cell stiffness. [2] The stiffness of ectoderm progenitor cells taken from zebrafish was compared to that of mesoderm and endoderm progenitors using AFM. Results showed that ectoderm cells had the highest stiffness, followed by mesoderm and endoderm progenitors. To measure if this stiffness was due to differential actomyosin activity, blebbistatin, a myosin inhibitor, was added to the cells and resulting measurements showed a universal decrease for all progenitor cell types. [53] In vitro cell sorting experiments using ectoderm and mesoderm cells showed ectoderm cells forming an inner sphere surrounded by mesoderm cells. The addition of cytochalasin D (actin inhibitor) and blebbistatin (myosin inhibitor) disrupted all cell sorting, suggesting that actomyosin dependent cell tension is required for progenitor sorting. [53] Additional cell sorting experiments have indicated that cells with high cadherin expression will migrate to the inner mass of a cell aggregate. [28] In these and other studies, it is important to consider the changes in the mechanical environment of individual cells as well as whole tissues.

2.3 Basement Membrane

The mechanical stiffness of the basement membrane may have an effect on the movements of the epithelial epiblast cells during gastrulation because substrate stiffness has been shown to affect cell migration. [61] [58] [46] The mechanical stiffness of the basement membrane has not been characterized, but matrix elasticity has been shown to effect differentiation, [32] migration, [82] [86] and proliferation. [86] In addition to research measuring the adhesion forces of the cell to various proteins, emerging studies measure the force with which cells adhere to gels of varying stiffness. Experiments using fibroblastic and epithelial cells lines as well as explants from rat hearts indicate that cells migrate and spread on stiff substrates, while they merge to form tissue like structures on soft substrates. [39] Stiffer substrates tend to induce a more organized

cytoskeleton and larger stable adhesions. [28] Matrix strain also has an effect on cell behavior; when cultured on polydimethysiloxane (PDMS) channels under compression, NIH 3T3 fibroblasts elongated along channels and formed actin filaments perpendicular to compressive strain. [14] Further, when cells are exposed to shear flow, actin filaments align themselves with the direction of shear stress. [76] As the substrate stiffness has been shown to affect cell behavior, a better understanding of development could be gained by characterizing the response of PS cells to varying substrate stiffness.

2.4 The Quail as a Model System

This study uses the Japanese quail *(Coturnix japonica)* as a model system to study gastrulation and cardiac differentiation. In addition to the imaging benefits of a translucent embryo that begins as a flat disc of cells that can be grown in a heat-controlled time-lapse microscopy setup, the quail has been used as a model system originating from Aristotle in the 4th century [36] and has long been considered a classical model of gastrulation. [96] It is the highest model system (an amniote, i.e. the fetus is contained in a fluid sac with an external membrane, including reptiles, birds, mammals) with high-throughput experiments that do not require the sacrifice of the mother. It is cheaply obtained, and matures faster than chick embryos, allowing for more experiments in a given period of study. The small egg size relative to chick eggs also allows for more and cheaper storage and incubation. Circulation was first discovered in unhatched chick eggs by William Harvey in 1628, [83] and the quail has an extensive history in the study of cardiac development, [52] particularly following introduction of the chick-quail chimera technique by Le Douarin, [56] which has contributed to fate-mapping experiments. [79]

Chapter III

SPATIOTEMPORAL MECHANICAL VARIATION REVEALS CRITICAL ROLE FOR RHO KINASE DURING PRIMITIVE STREAK MORPHOGENESIS[1]

3.1 Introduction

During gastrulation in amniotes, including reptiles, birds, and mammals, undifferentiated cells in the epiblast move collectively toward the embryonic midline and organize into a structure known as the primitive streak a critical early morphogenetic process that results in the formation of the three primary germ layers: endoderm, mesoderm, and ectoderm. Epithelial-to-mesenchymal transition (EMT) of endodermal and mesodermal precursors and their subsequent ingression through the primitive streak sets the stage for organogenesis. As Lewis Wolpert famously remarked, "It is not birth, marriage, or death, but gastrulation which is truly the most important time in your life." [93] Molecular studies over the past couple of decades have identified critical signaling pathways required for primitive streak formation and maintenance however, the underlying biophysical mechanisms and cellular driving forces are not known and are still actively being investigated. [15] [16] [17] [110] [118] While it has been shown that actomyosin contractility plays a fundamental role in gastrulation movements in anamniote (fish, amphibians) and lower model organisms ranging from Drosophila (ventral furrow invagination) to Xenopus (blastopore formation),

[1]HENKELS J, OH J, XU W, OWEN D, SULCHEK T, ZAMIR E. *SPATIOTEMPORAL MECHANICAL VARIATION REVEALS CRITICAL ROLE FOR RHO KINASE DURING PRIMITIVE STREAK MORPHOGENESIS.* ANN BIOMED ENG. 2013 FEB;41(2):421-32. DOI: 10.1007/S10439-012-0652-Y. EPUB 2012 SEP 7. PMID: 22956163

surprisingly, its specific role during primitive streak formation remains somewhat of an enigma. In anamniotes, actomyosin-driven apical constriction − a characteristic morphogenetic process which drives bending, invagination, and involution of epithelial sheets in embryos [18] [74] − is widely considered to be the primary morphogenetic initiator of mesendodermal internalization. The current leading models of avian primitive streak formation mostly implicate cell migration driven by chemotaxis [15] [20] [87] [88] and/or cell-cell intercalation. [110] However, in our understanding of amniote gastrulation, additional biophysical mechanisms are at play. We recently showed that epiblast cells essentially move in concert with their underlying basal lamina, [118] thus, suggesting to us that the cell trajectories interpreted by other groups as evidence for cell migration ("crawling" of individual cells), instead represent large-scale tissue-level movements like those generally thought to be driven by apical constriction in Drosophila or Xenopus embryos. It is well known in mechanics that the apparent stiffness of a body in tension increases over its reference (non-stressed) state. [117] This fact has proven to be useful in biophysical studies of cell mechanics, in which actomyosin contractility results in increased (internal) cellular tension, sometimes called "pre-stress." [5] [80] [112] Many previous studies have investigated the changing mechanical properties in embryonic processes, for example, sea urchin invagination, [22] gastrulation, [70] and neural tube elongation and closure [122] in Xenopus, and we previously probed mechanical properties of the looping chick heart. [116] Surprisingly, to our knowledge, there are no studies of spatial or temporal changes in mechanical properties of the epiblast or primitive streak in amniote embryos, even though such data could potentially yield important insight into the biophysical process of gastrulation. In this study, we present for the first time data concerning the mechanical properties of the avian epiblast and primitive streak, which suggest that primitive streak formation and epiblast convergence towards the primitive streak are driven in large part by actomyosin contractility. Our atomic force microscopy (AFM) data

show that the primitive streak stiffens during early gastrulation and this increase in stiffness requires Rho kinase-mediated actomyosin contractility. Furthermore, cell tracking data from time-lapse imaging experiments suggest that actomyosin contractility is needed for normal convergence of the epiblast cells towards the midline of the embryo during gastrulation. Taken together, our data represent a leap forward in our ability to answer Trinkaus fundamental question, "What are the forces that shape the embryo?" [106]

3.2 Materials and Methods

3.2.1 Avian embryo preparation

Quail eggs (Coturnix Coturnix Japonica, Ozark Eggs, Stover, Missouri) were incubated at 38 °C for 2-3 hours. The embryo was dissected from the egg, mounted on filter paper rings, placed ventral side up on a semi-solid mixture of agar/albumen (egg whites) (modified after the method of New [13] [74]), and then incubated further at 38 °C until Hamburger and Hamilton [40] stage 1 (HH1) or stage 3 (HH3) depending on the experiment. Although the Eyal-Giladi [33] staging system divides the pre-primitive streak avian embryo into stages X − XIV according to the amount of hypoblast tissue, for the purpose of this study, we characterized freshly-laid quail eggs as HH1 because the hypoblast was removed for our experiments. (See following section for details.)

3.2.2 AFM sample preparation

Preliminary experiments were conducted on whole embryos; however, undulations in the embryo prevented reliable readings given the working distance of the AFM. Explanting tissue allowed for a reliable analysis of specific embryo regions of interest in a stress-free state, that is, outside of the tensile environment in the embryo at these early stages (see Results). Numerous methods were initially attempted to hold tissue samples stable for AFM testing. This proved to be quite challenging, due to the

small size, as well as the extreme fragility of the embryonic tissue. Several adhesives, including poly-L-lysine and fibronectin, which are routinely used for single cell experiments, proved to be too weak. The method that we finally utilized is as follows. In a glass-bottomed 50-mm plate, an array of 400-μm diameter PDMS microwells (see subsequent section for microfabrication details) were self adhered to the glass surface. The dishes were filled with serum-free media (RPMI 1640 + 1X ITS + 1% P/S/L-glut). HH1 and HH3 quail embryos were placed in PBS containing Mg++/Ca++. A 300-μm-diameter tissue biopsy punch was used to explant (1) anterior (ANT1), (2) central (CEN1), (3) Kollers sickle (KOL1), and (4) lateral (LAT1) epiblast regions of HH1 embryos and (1) anterior (ANT3), (2) anterior primitive streak (APS3), (3) posterior primitive streak (PPS3), and (4) lateral (LAT3) regions of HH3 embryos (Figure 2).

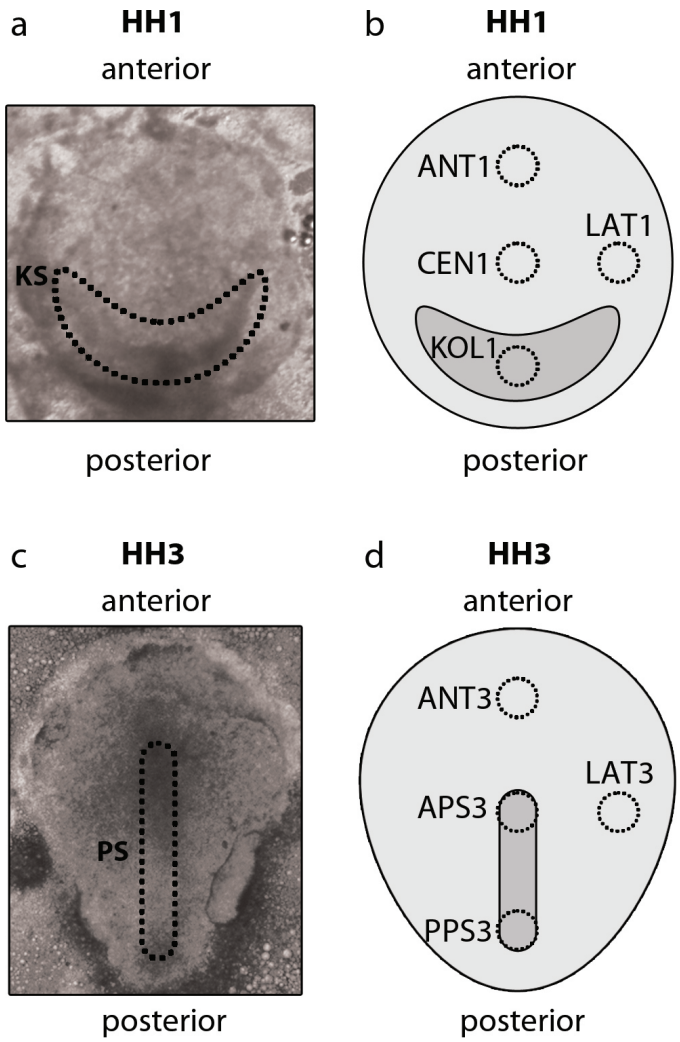

Figure 2: Schematic of quail embryo at HH1 and HH3

Brightfield images of HH1 (a) and HH3 (c) quail embryos. A tissue biopsy punch was used to remove 300-μm-diameter regions of HH1 (a,b) and HH3 (c,d) quail embryos for AFM analysis. KS, KOL = Kollers sickle. PS = primitive streak. ANT = anterior epiblast. CEN = center of epiblast. LAT = lateral epiblast. APS = anterior primitive streak. PPS = posterior primitive streak.

Because the hypoblast is adhered to the lateral edges of the epiblast at HH1 (and not the bulk of the epiblast where samples were explanted), the hypoblast layer separated easily from the epiblast layer after explantation with the biopsy punch. For

each embryo, explants from each region were carefully placed with a pipette in individual PDMS microwells to enable comparison between specimens as rapidly as possible. Next, a 3-mm diameter, 20-μm thick copper TEM 150 mesh with approximately 100-μm grid spacing (Structure Probes, Inc., West Chester, PA) was placed over all samples, thus gently holding them in the microwells while at the same time allowing access of the AFM probe (Figure 3).

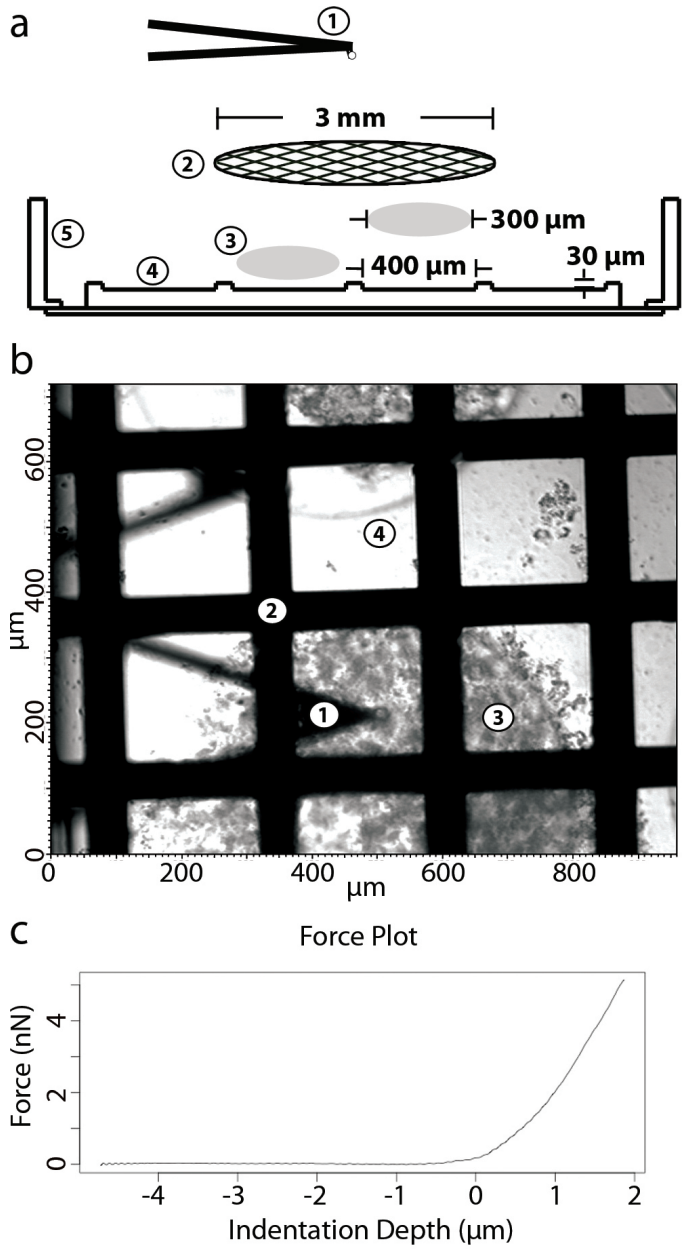

Figure 3: Atomic force microscopy sample preparation and experimental setup

A schematic of AFM setup is shown in (a) and consists of the following: (1) AFM cantilever; (2) TEM mesh used to secure (3) tissue explants; (4) PDMS microwells used to contain samples; (5) glass bottom dish. (b) Shown is a still video frame from an AFM force-measurement experiment, with label numbers corresponding to schematic from (a). (c) Sample force versus indentation curve for one indentation.

Initial indentation tests were conducted to verify that the TEM mesh did not affect the measured tissue stiffness. For sample transfer to the AFM lab, tissue explants were further held in place using a polycarbonate filter (pore size 20 μm), 13-mm diameter, with a thin layer of vacuum grease at the edges to hold it in place over the copper mesh.

3.2.3 PDMS microwell fabrication

Microwells (400-μm diameter) used to hold the embryo tissue for AFM were fabricated by a replica molding method. A template used to create a master PDMS mold was fabricated by standard photolithography. The general process was as follows. (1) A silicon wafer was cleaned with Piranha solution ($4(H_2SO_4)$:$1(H_2O_2)$) for 10 minutes to remove any organic compounds, cleaned with hydrofluoric acid [26] for 10 seconds to remove the oxide layer, and rinsed with DI H_2O for 10 minutes. (2) The wafer was spin-coated with SU-8 (SU-8 2035; Microchem, Newton, MA) to a thickness of 30 to 40 μm; (3) soft-baked to remove solvent by gradually increasing and decreasing temperature (55 °C to 95 °C with 2 °C/min ramping) and cooled at room temperature at least for 10 minutes; (4) exposed to UV (365 nm) light through a film mask; (5) hard-baked on the hot plate to cross-link the SU-8 resin by gradual temperature change as in the soft-bake process; (6) cooled again on the room temperature for 10 minutes; (7) developed in SU-8 developer (Microchem) to remove the unexposed photoresist; (8) rinsed with IPA (Isopropanal) to verify development completeness and rinsed again with DI H_2O; and (9) dried with a nitrogen gun. The template created by photolithography was (1) blown by the nitrogen gun to remove as much dust as possible on the surface; (2) coated with PDMS pre-polymer (Sylgard 184 kit, Dow Corning) with 10:1 (wt%) ratio of base and curing agent; (3) placed in a vacuum chamber to remove air bubbles in the pre-polymer; (4) cured at 110 °C for 2 hours; and (5) peeled from the template to produce the final PDMS microwells.

3.2.4 Atomic force microscopy

Atomic force microscopy (AFM) is a sensitive device that measures force and displacement simultaneously and has been used in such fields as nanoindentation and biophysics. [4] [8] The AFM used in our experiments was MFP-3D from Asylum Research (Santa Barbara, CA). A Nikon Ti inverted optical microscope was combined with the AFM to visualize the sample and cantilever simultaneously during measurements. The probes used were MCST-AUHW from Veeco (Plainview, NY). To simplify the contact geometry and minimize the lateral strain of the sample during indentation, the cantilever was modified by attaching a rigid polystyrene microsphere of 15-μm diameter, which did not deform during indentation. Measurements were taken in a liquid media environment at room temperature in a 50-mm fluorodish from World Precision Instruments (Sarasota, FL). The AFM probe was completely immersed in the culture media during measurements. The cantilever was calibrated on the glass bottom of the fluorodish using thermal vibration method [63] with the resultant thermal spectrum fitted with Lorentzian function to determine the spring constant. The force versus indentation curve in each measurement was analyzed with Hertz model [47] [113] to obtain the Young's modulus of the sample at the location of indentation. The Hertz model is widely used in contact mechanics research. [47] [48] The model was first derived for the normal contact between two deformable spheres and has been adapted for other contact geometries as well. The mathematical expressions of the Hertz model for two deformable spheres are as follows:

$$\alpha^3 = \frac{3PR}{4E*}$$

$$\delta = \left(\frac{9P^2}{16RE*^2}\right)^{1/3}$$

where α is the radius of the contact region between the indenter and the sample, δ is the indentation into the material, P is the loading force, R is the effective radius

of curvature defined as

$$\frac{1}{R} = \frac{1}{E_1} + \frac{1}{E_2}$$

$E*$ is the apparent Young's Modulus defined as

$$\frac{1}{E*} = \frac{1-\nu_1^2}{E_1} + \frac{1-\nu_2^2}{E_2}$$

where ν_1, ν_2 are Poissons ratio for the material and the subscripts denote the two contacting bodies. The embryo sample can be considered flat as compared to the microsphere, which means R simplify reduces to R_1, the radius of the microsphere used in this study.

The moduli were derived from multiple indentations. Five locations were selected on each explant—within each location, a force measurement was repeated 5 times. We found that the variability between different locations on an explant was much greater than the variability between repetitions on the same location. Therefore, we averaged the Young's modulus over 5 repetitions in each location, thus yielding 5 values for each explant.

3.2.5 Pharmaceutical inhibition of Rho Kinase by Y-27632

The Rho kinase (ROCK) inhbitor, Y-27632 (Tocris Bioscience, Ellisville, MO), was used in AFM, whole embryo culture, and time-lapse imaging experiments to examine the effect of decreased contraction via the ROCK pathway. For the AFM samples, embryos were incubated in 100 μM Y-27632 + serum free media (RPMI 1640 + 1X ITS + 1% P/S/L-glut) for 1 hour at 37 °C. To examine the effects of ROCK inhibition on cellular movements using time lapse imaging, embryos were initially transfected with pCAG-GFP and returned to the agar/albumin culture plates for 2-3 hours until robust expression was observed. Next, embryos were placed on freshly prepared culture plates containing 100 μM Y-27632 and placed in our custom computer-controlled time-lapse microscopy setup. Control and treated embryos were imaged for up to 5 hours. For the whole embryo culture experiments, Y-27632 was

dissolved in the agar/albumen media and pre-streak (HH1) embryos were incubated for 12 hours (overnight).

3.2.6 Electroporation

Plasmid DNA (pCAG GFP; AddGene #11150) was prepared for electroporation by combining an endotoxin-free concentrated stock of plasmid with Solution A (1 mM $MgCl_2$, 0.2% Phenol Red in PBS + 1.0 mL 10x PBS + 10.0 μL 1.0 M $MgCl_2$S solution; Sigma Cat. #M-1028 + 5.0 mL 0.4% Phenol Red solution in H_20, Phenol Red, Fisher Cat. #P-391) producing a final concentration of 1 μg/μL. A glass micropipette was pulled (Narishige Model PL-10), cut with forceps, and filled with plasmid ($\sim$ 2 μL). A micropipette holder was secured in a micromanipulator (Narishige). The top electrode (Protech International CUY700P5E) was fixed in a second micromanipulator (Narishige), and the electroporation chamber (Protech International CUY700P1L) containing the bottom electrode was filled with Hank's media and centered on the microscope (Leica MZ16F) stage. The terminals were attached to the electroporator (Intracel TSS20 Ovodyne Electroporator). Embryos were transferred to a Millicell® cell culture insert (PICM03050) filled with semi-solid culture media, dorsal side up. The vitelline membrane was pierced with the micropipette and plasmid injected with the microinjector (Harvard Apparatus Medical Systems Research Products PLI-100). Then, the micropipette was removed and the top electrode was lowered to the embryo surface; a drop of 15 μL Hank's media was used to dissipate surface tension. The embryo was then electroporated at 4 V with four square pulses of 40-ms duration (900 ms between pulses). Embryos were then washed in PBS and transferred (dorsal side down) to a new culture dish for incubation at 37 °C until expression was seen.

3.2.7 Time-lapse microscopy

A complete description of the time-lapse microscopy system is given elsewhere. [21] [84] Briefly, a Leica DMI6000 inverted epiuorescent microscope with a motorized

BioPrecision stage (Ludl, Hawthorne, NY) controlled by a modular MAC 5000 (Ludl) automation controller system and CCD digital camera (Hammamatsu Orca) captured grayscale images at multiple focal planes once every 6 min for the duration of the experiment. Image processing consisted of collapsing focal planes and outputting a single focused and "mosaicked" wide-field image per embryo per time point.

3.2.8 Cell tracking

Cells were manually tracked using ImageJ, a freely-available open source image-processing program. An ImageJ plug−in called "Running Z-Projector" (`http://valelab.ucsf.edu/~nico/IJplugins/Running_ZProjector.html`) was used to create cell trajectories for 5 consecutive image frames (the equivalent of 30 min of experiment time) at the 1-hour time point, and 30 cells for each embryo were manually tracked using the built-in measurement tool. The x− and y− coordinates of the cells were then imported into Matlab (Mathworks, Natick, MA) and the calculated cell velocities (in μm/min) were fit by a thin plate spline using the Matlab spline toolbox. Control and drug-treated samples were then averaged to produce an "ensemble" velocity map for each group, which allowed for simpler comparison.

3.2.9 Statistical analysis

All statistical analyses were performed in R (`http://www.r-project.org`), a free software environment for statistical computing and graphics. A one-way omnibus ANOVA test was completed to ascertain significant differences between the Young's modulus within the regions of the HH1 and HH3 embryo groups. Significant differences were found within the HH3 regions ($p<0.001$), therefore, an ANOVA pairwise comparison test was completed on HH3 data. To take into account variation between individual embryos, a Friedman Test, one version of the rank sum test, was used. Each of the four regions under consideration within individual embryos (ANT1, CEN1, LAT1, KOL1, and ANT3, APS3, PPS3, LAT3) was ranked based on stiffness.

However, in order to use the Friedman Test for nonparametric data and assign ranks for each region within an embryo sample, missing data from our AFM measurements had to be imputed.

Missing data from different regions within the same embryo could occur due to the difficulty of handling samples and fragility of the explants, or on occasion irregular force curves from the AFM indentations due anomalous causes, such as insufficient immobilization of the embryo or possible contact of the probe with the embryo at locations besides the tip. In some cases, the samples were not well constrained by the TEM trap and moved during the indentation test, thus resulting in unreliable force curves. Force curves that were deemed unreliable were thrown out. There were a total of 5 missing data points for HH1 (out of 24 explants isolated from 6 embryos), 2 missing data points for stage 3 controls (out of 36 explants isolated from 9 embryos), and 2 missing data points for stage 3 embryos treated with Y-27632 (out of 40 explants isolated from 10 embryos).

Missing data can be classified in several ways. In the best case, data are missing completely at random (MCAR), which means there is no correlation between the treatment groups and the missing data. If there is a correlation between missing data and characteristics of the treatment group, the data are characterized as missing at random (MAR). [3] In our study, the data were not missing due to any characteristic of any particular group of samples; hence, the data was considered MCAR.

There are several ways to overcome missing data. First, samples with incomplete data could be excluded. However, in most cases including ours, this method would lead to statistically insignificant results and exclude a large percentage of good data. Other methods of imputation include case analysis, the missing-indicator method, mean imputation, single imputation, and multiple imputation. Case analysis and missing-indicator method require a former precedent to be in place, and none exists

for this study, since, to our knowledge, there are no previous data for primitive streak-stage mechanical properties in avian embryos. We did not use mean imputation because it has been shown to produce biased results. [29] In single random imputation (SRI), a data point is randomly selected from the same data set to fill in the missing value and a single p-value is calculated. In theory, every time SRI is done, a different p-value is generated based on the random data point selected, and depending on the particular (random) data point selected, the p-value may vary considerably. Multiple random imputation (MRI) consists of repeated selection of random data points from the set, which are averaged to arrive at a single imputed replacement value for the missing data point. Essentially, MRI can be considered "bootstrapping" approach to impute a single data point, and then the filled-in data set is used to generate, for example, a single p-value from a statistical test. We developed a more robust version of statistical inference for data sets with missing values. The objective of our method is to determine confidence intervals for the p-values. Our method is to iterate SRI 10,000 times and run a statistical test (Friedman test) each time. We then compute the χ^2 values (the statistical output parameter of the Friedman test) and corresponding p-values for each of the 10,000 SRI iterations, which results in a bootstrapped p-value distribution.

Finally, to discern statistical differences between regions we used the Friedman Comparison test. Both SRI and MRI (using 10,000 imputation iterations) were completed on the HH1, stage 3 controls and Y-27632-treated data sets. Next, the Friedman Comparison Test was performed on both SRI and MRI data sets.

3.3 Results

3.3.1 Primitive streak mechanically stiffens relative to other epiblast regions during its formation

As described in the Methods, we extracted small circular tissue punches from various spatially separated regions of pre- and post-primitive streak embryo stages (HH1 and

HH3) and used atomic force microscopy (AFM) to measure the Young's modulus of these different regions. To be clear, in terms of the mechanics, technically, stiffness should account for both geometric and mechanical properties of the sample. In this study, since all samples were practically identical circular-shaped punches of similar thickness (i.e. geometry was held constant across different samples), and since the indentation was considered small (much less than 1/10 of the tissue thickness), the Young's modulus calculated from the analytical AFM experimental model (described in Methods) actually represents an intrinsic ("true") elastic measure of tissue mechanical properties that is often simply referred to as "stiffness." In linear elasticity, the famous Hookes Law relates stress σ (force per area) to strain ϵ (deformation) through the Young's modulus (E): $\sigma = E\epsilon$. For example, given more force applied to a body (left side of equation) of identical shape and size, the body with a larger Young's modulus will undergo less strain. By probing the epiblast tissue from different regions, we can identify whether a given region becomes stiffer (i.e. E increases) over time and/or relative to other regions.

It is also important to note that in this study we isolated tissue samples from the embryo before probing for stiffness, although a previous study on older somite-stage embryos probed whole embryos with a glass needle. [1] We made this choice because while it is intact and adherent at its edges to the vitelline membrane, the epiblast at this stage appears to be under considerable tension as gastrulation proceeds. Such tension—generally referred to as "residual stress" by biomechanicians—can be revealed by making microsurgical (linear) cuts in the tissue and measuring the size of the resulting "wound" opening. From previous (unpublished) experiments in our lab, it appears to us that this tension actually increases over time, starting with virtually no tension (edges of wound remain virtually closed) at HH1. The importance of this observation is that increasing tension alone (e.g. think of inflating a balloon or stretching a rubber band) can create the appearance of increased stiffness, which

is not necessarily associated with any change in Young's modulus. Therefore, by removing the tissue samples from the embryo, we were able, to probe the inherent or "true" material behavior of each region without using more complicated analysis that would be necessary otherwise to model the presence of residual stress in the intact embryo. [119] [117] Furthermore, although handling such small tissue punches eventually required us to develop a specialized microfabricated holding chamber, our initial attempts to perform the measurements on whole embryos at such early stages proved to be even more difficult, since the large-scale geometrical undulations and extremely large aspect ratio (width-to-thickness) of the embryo prevented stable and consistent AFM measurements, thus providing us with even more incentive to develop our ex vivo testing protocol.

Epiblast tissue samples were isolated from the anterior (ANT1), central (CEN1), Kollers Sickle (KOL1), and lateral (LAT1) regions of HH1 embryos, and anterior (ANT3), anterior primitive streak (APS3), lateral (LAT3), and posterior primitive streak (PPS3) regions for HH3 embryos (Figure 2). For each sample, AFM measurements were taken 5 times consecutively in each of 5 different locations within each individual explant (Figure 4).

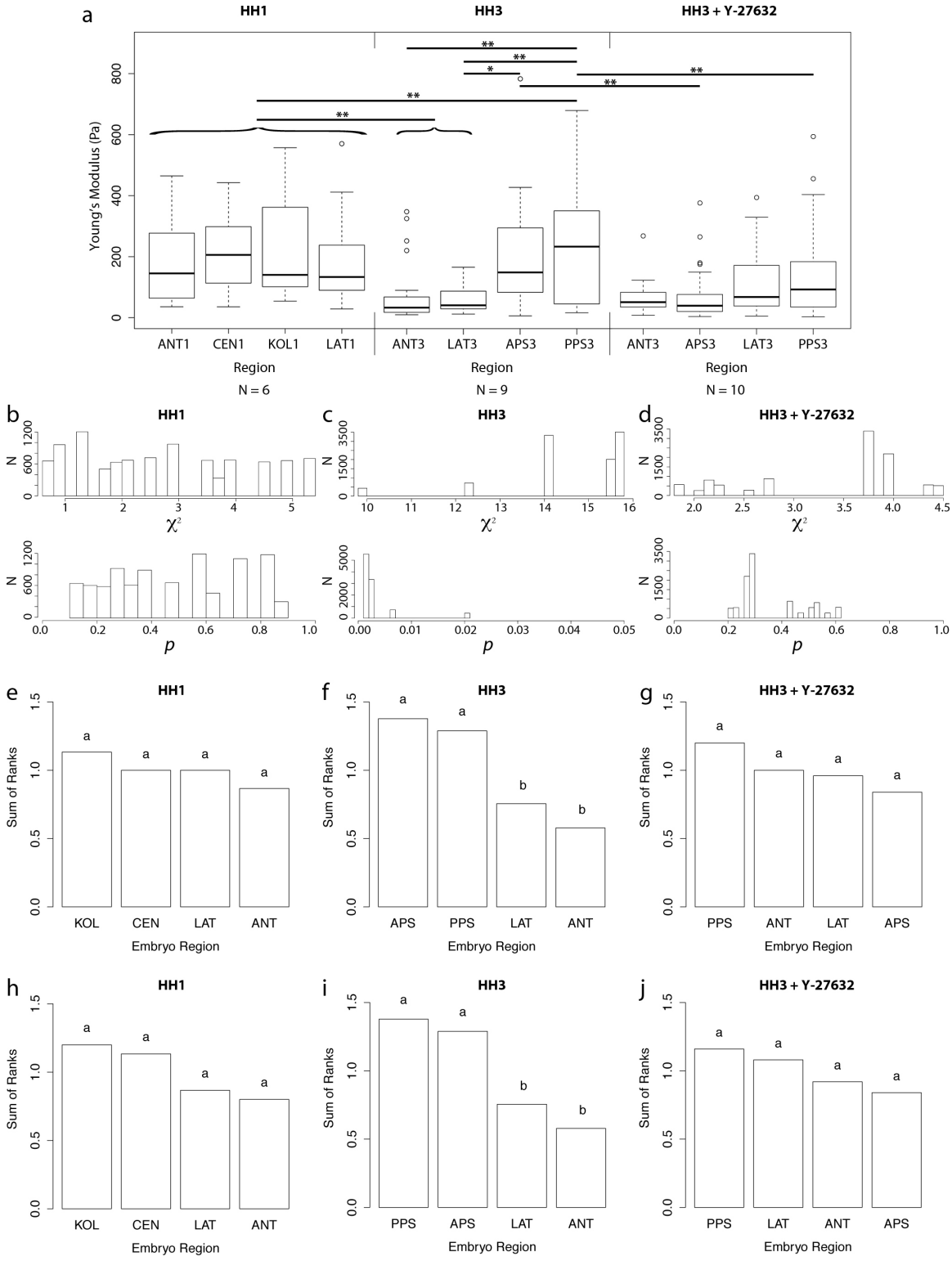

Figure 4: Caption next page.

Figure 4: (Previous page.) Mechanical properties of epiblast in HH1 and HH3 embryos (a) Young's modulus of HH1 (left; N=6), HH3 (middle; N=9), and HH3 embryos treated with Y-27632 (right; N=10). The boxes represent the 25th to 75th percentiles, and the heavy line represents the median. Whiskers represent the top and bottom quartiles of the data. Outliers (less than or greater than 1.5 times the inner quartile range) are denoted by open circles. Heavy lines indicate statistical significance according to a paired t-test (* = $p<0.05$; ** = $p<0.001$). (b,c,d) Bootstrapped Friedman tests were used to generate a distribution of p-values (see Methods). Note that the distribution of p-values was always found to be significant ($p<0.05$) for HH3 controls, and never for HH1 or HH3+Y-27632 embryos, thus confirming the validity of our imputation method. (e,f,g) Results from Friedman comparison tests with missing data imputed by single random imputation (SRI). Different letters indicate groups that are significantly different ($p<0.01$). (h,i,j) Results from Friedman comparison tests with missing data imputed by multiple random imputation (MRI). Different letters indicate groups that are significantly different ($p<0.01$).

We investigated whether there are spatial differences in Young's modulus between the various anatomical regions of the epiblast in HH1 and HH3 embryos. Because it was not known a priori whether intra-embryo (within individual embryos) or inter-embryo (between different embryos) variation would be a larger factor in the analysis, we used both parametric (population mean and variance) and non-parametric tests (ranks) to make comparisons. First, we use a standard ANOVA test that accounts for the variance of the entire sample population (i.e. embryos grouped by epiblast region). We found that for HH1 embryos, there was no statistical difference between regions according to a one-way omnibus test ($p\sim0.90$; Figure 4a). However, there was a statistical difference between regions in HH3 embryos ($p<0.001$). To determine which region(s) were significantly different from each other, we performed a pairwise

t-test (Figure 4a). Specifically, the Young's modulus of the posterior primitive streak (PPS3) is significantly greater than that of the anterior epiblast (ANT3; $p<0.001$) and lateral epiblast (LAT3; $p<0.001$). The anterior primitive streak (APS3) is significantly stiffer than the lateral region (LAT3; $p<0.05$), but not the anterior portion of the epiblast (ANT3). No statistically significant difference was found between the anterior primitive streak (APS3) and posterior primitive streak (PPS3). Finally, the anterior epiblast (ANT3) and the lateral epiblast (LAT3) were not found to be statistically different, in terms of Young's modulus.

A bootstrapped version of the Friedman test was used to look for differences between regions within embryos that may not be detected by ANOVA, due to large variation between different embryos (see Methods). The distribution of p-values given by the bootstrapped test confirms that there are no statistically significant differences between the defined regions of the HH1 embryos (Figure 4b-d), and there are statistically significant differences within the HH3 data (Figure 4c). Friedman comparison tests on HH3 embryos using either single random imputation or multiple random imputation (MRI) showed that the anterior primitive streak and poster primitive streak were significantly stiffer relative to the lateral and anterior regions of the epiblast (Figure 4f,i).

Next, we investigated whether there are temporal changes in Young's modulus between stages 1 and 3. We lumped together the data from all regions for HH1, since they were not statistically different from each other. The Young's modulus of the posterior primitive streak (PPS3) was increased by approximately 50% compared to the HH1 data ($p<0.001$). The anterior primitive streak was not found to be statistically different from the HH1 epiblast data. One of the most surprising results of this study is that anterior (ANT3) and lateral (LAT3) regions of the stage 3 epiblast, which were lumped together since they were not statistically different from each other, were significantly softer by a factor of about 3 compared to the HH1 data

($p<0.001$). These data suggest that genetically-regulated tissue relaxation may be as essential as tissue contraction for morphogenetic tissue movements.

3.3.2 Rho Kinase Contributes to Increased Stiffness of Primitive Streak

To investigate whether actomyosin contractility is necessary for primitive streak formation, we treated pre-primitive streak embryos (HH1) with Y-27632, a pharmaceutical inhibitor of Rho Kinase (ROCK), for 12 hours. The control embryos all developed normal primitive streaks and were approximately HH3 after 12 hours (N=12). In contrast, 10 of 12 Y-27632 treated embryos failed to develop primitive streaks and the appearance of the epiblast was essentially unchanged from HH1 embryos (Figure 5).

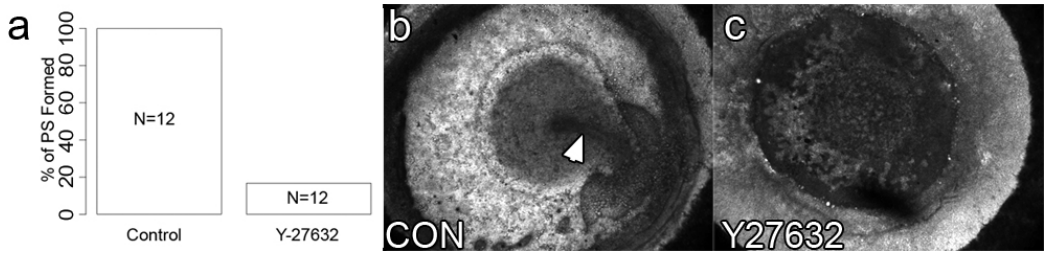

Figure 5: Effects of ROCK inhibition on primitive streak formation
(a) Embryos incubated with ROCK inhibitor (Y-27632) for 12 h failed to form primitive streaks compared to untreated controls. (b,c) Representative brightfield images of a control HH3 embryo and a Y-27632-treated embryo that did not form a primitive streak.

To determine the contribution of actomyosin contractility to stiffness in the different regions of the primitive-streak stage epiblast, we treated HH3 embryos with Y-27632 for 1 hour at 100 μM. Following treatment, 300-μm-diameter epiblast tissue punches from each of the regions (ANT3, APS3, PPS3, LAT3) were explanted and the Young's modulus was measured using AFM. We found that the Young's modulus of the anterior and posterior primitive streak treated with Y-27632 was approximately

3-fold and 2-fold lower, respectively, compared to untreated controls ($p<0.001$; Figure 4a). There was no statistical difference found between the anterior or lateral regions of Y-26732 embryos compared to control embryos. Moreover, both one-way ANOVA and our modified bootstrapped version of the Friedman test (see Methods) showed that there are no significant differences in the Young's modulus between any of the HH3 embryo regions following Y-27632 treatment (Figure 4 c,f,i,l), thus strongly suggesting that actomyosin-driven cell contraction causes an increase in primitive streak stiffness relative to other regions of the HH3 epiblast during gastrulation. A control experiment was completed to test for viability following Y-27632 treatment. HH3 embryos were treated with Y-27632 for 1 hour at 100 μM, then transferred to agar/albumen Y-27632-free plates. At 0, 3, and 12 h time points, a live−dead nuclear assay indicated no difference between the viability of treated and untreated embryos (data not shown).

3.3.3 Rho Kinase Inhibition Reduces Epiblast Cell Convergence towards the Primitive Streak

We investigated the role of ROCK-mediated actomyosin contractility in epiblast movements in HH3+ embryos. Whole embryos were first electroporated with pCAG-GFP to fluorescently label the cells and subsequently treated with 100-μM Y-27632. The embryos were incubated in our time-lapse imaging setup (see Methods), and fluorescent and brightfield images were captured every 6 minutes, and then processed to generate time-lapse movies for motion analysis. Thirty cells from each embryo (N = 7 controls; N = 13 Y-27632-treated) were manually tracked over five time points (24 min total) starting at 1 hour into the experiment.

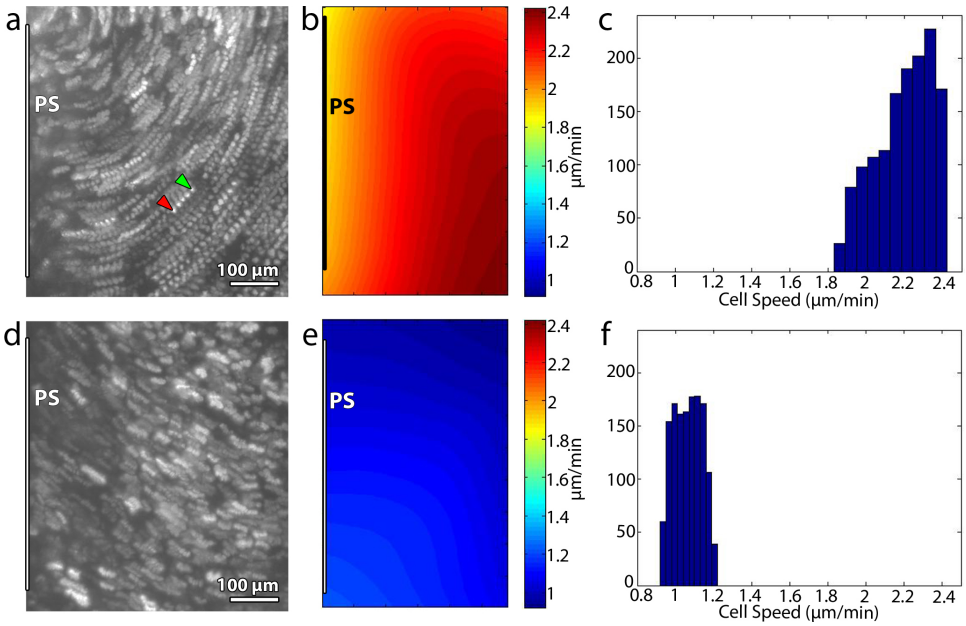

Figure 6: ROCK inhibition diminishes epiblast cell convergence to midline

Z-projections from time-lapse imaging experiments show that in control embryos, cells move more rapidly toward the primitive streak (a) than embryos treated with 100-μM Y-27632 (d). Primitive streak (PS) is shown at the left of panels a, b, d, and e. Arrowheads in (a) denote the beginning (green) and end (red) of a single cell trajectory over 25 minutes. Ensemble velocity contour maps (b,e) and histograms (c,f) confirm that cell velocity was significantly reduced in treated embryos (N=13) compared to controls (N=7; see Methods for details of data analysis).

Upon inspection of the length of the cell trajectories, it appeared that the treated cells (Figure 6d) had a lower velocity then the control cells (Figure 6a). To quantify this phenomenon, individual cell velocities for each embryo were fit with a spline function and used to make a composite or "ensemble" velocity map averaging all measurements for control (Figure 6b) and Y-27632 treated embryos (Figure 6e). Our data showed that there was an approximately two-fold decrease in cell velocity after ROCK inhibition (Figure 6c,f), and the difference was statistically significant ($p<0.001$).

3.4 Discussion

Our data suggest a much more critical role for ROCK-mediated actomyosin contractility in primitive streak formation and epiblast convergence in amniotes than has previously been reported. Culturing pre-primitive streak embryos overnight (12 h) in media containing Y-27632 blocked primitive streak formation in 10 out of 12 embryos. This dramatic effect of ROCK inhibition contradicts a previous study that reported 13/15 embryos developed normal primitive streaks when treated with Y-27632; [18] however, the authors of that study did not report any concentration data, and we speculate that they used a much lower concentration than was used in our study. They also used blebbistatin, a myosin II inhibitor, and found no significant perturbations in epiblast movements, but the reported concentration was only 5 μM, which we have found needs to be used upwards of 200 μM before effects are even noticeable (unpublished data). The requirement for much higher concentrations of pharmaceutical inhibitors in semi-solid avian culture has been noted previously in a study of early heart development. [112] Furthermore, previous studies of actomyosin contractility in Xenopus embryos have also reported using a range of concentrations of pharmaceutical inhibitors similar to the current study. [57] Therefore, it is not surprising to us that the previous study by Chuai [18] did not find any effect.

The observed effects of ROCK inhibition on primitive streak formation could be due to signaling pathways other than those directly involved in actomyosin contractility. For example, ROCK is important for cell adhesion and proliferation. It is possible that during the relatively long incubation time needed to test whether the primitive streak forms, these and other downstream pathways may have been perturbed. Our hypothesis that the main effects of ROCK inhibition on primitive streak formation are specifically due to a reduction in actomyosin contractility lead us to make the following predictions: 1) The primitive streak is stiffer than the pre-primitive streak stage epiblast due to increased actomyosin contractility; 2) The primitive streak is

stiffer than other regions of the stage 3 epiblast due to localized increase in actomyosin contractility; 3) Primitive streak stiffness will decrease very rapidly after ROCK inhibition; and 4) Epiblast convergence to the embryonic midline will be reduced very rapidly after ROCK inhibition. Each of these predictions was tested, and taken together the results support our overall hypothesis that each "wave" of cells that progresses through the primitive streak constricts and then ingresses, and the subsequent wave of cells constricts and ingresses. In this way, each individual cell constriction at the primitive streak contributes to the overall tissue movement of the epiblast toward the primitive streak.

Our AFM data show that the Young's modulus of the posterior primitive streak is approximately 50% greater than the HH1 epiblast; interestingly, however, the anterior primitive streak was not found to be significantly different. We speculate that the reason for the difference between the anterior and posterior portions of the primitive streak results is due to a gradient of actomyosin contraction along the anterior-posterior axis of the primitive streak. Our cell tracking data indicate that epiblast cells move faster toward the posterior primitive streak compared to the anterior primitive streak (Figure 6), which may be the result of a gradient of actomyosin contractility. We suggest that these data could be input into a mathematical model of epiblast morphogenesis similar to a recent model proposed by Sandersius, [87] except cell movement would be driven by an actomyosin contractility gradient instead of a chemotactic gradient.

It could be that the increased stiffness of the primitive streak at HH3 is indicative of an overall increase in stiffness in the embryo as a result of tissue differentiation, but our data do not support this idea. Instead we find that the anterior and posterior portions of the primitive streak are both stiffer than the anterior and lateral portions of the HH3 epiblast.

A surprising finding in our AFM data is that the Young's Modulus of the anterior

and lateral regions of the HH3 epiblast is 3-fold lower than the HH1 epiblast. This unexpected result could be due to remodeling of cellular architecture, which results in a decrease in mechanical stiffness in these regions. It appears that a decrease in cell stiffness outside of the primitive streak accommodates the required movements of epiblast morphogenesis. In other words, non-primitive streak epiblast cells actively lower their compliance to "go with the flow" during this dynamic stage of development. Genetically-regulated "tissue softening," whether it works in concert with tissue stiffening or alone, is likely a major component in determining specific morphogenic outcomes. In Xenopus, it has been shown that the mechanical properties of the tissues surrounding the apically-constricting blastoporal cells determine the resulting shape changes and movements of surrounding tissues. [41]

Our results of velocity mapping of cell convergence towards the primitive streak showed that the cells move more quickly in the lateral epiblast than just outside the primitive streak, that is, they move faster further away from the primitive streak and then decrease in velocity near the primitive streak. In addition, our AFM results showed that the *faster-moving lateral region* was significantly *softer* than the *slower moving tissue* taken from near the primitive streak, which was *stiffer* than the rest of the embryo. These results support our hypothesis that tissues *soften* during development to move more *quickly* in formative developmental processes, whereas *stiffer* tissues are more *resistant to large-scale movement*, as was seen in the velocity of cells in the stiffer region of the primitive streak.

The data from our AFM and time-lapse imaging experiments show that Y-27632 has immediate effects on the embryo. Following ROCK inhibition, the stiffness of the primitive streak dramatically decreases, however, the anterior and lateral regions do not exhibit a decrease in stiffness. The overall result is that the difference in stiffness between the different regions was abolished after treatment. ROCK inhibition also caused significant phenotypic changes almost immediately, as evidenced by a 50%

reduction in the velocity of cell convergence toward the primitive streak.

Current models of amniote gastrulation and, specifically, primitive streak morphogenesis, do not take into account mechanical properties of the embryo, let alone the spatiotemporal variation of mechanical properties that we have shown here. In general, biomechanical properties are due to a combination of active and passive processes at the cellular and sub-cellular level. It has previously been shown in other widely used model organisms, including the sea urchin and Xenopus, that changes in both active and passive mechanical properties are critical for normal developmental processes. Our data strongly suggest that an increase in primitive streak stiffness during early gastrulation is due primarily to an active process driven by actomyosin contractility and requires ROCK. In other words, what we measure as an increase in tissue stiffness with the AFM, is not simply correlated with an active process, but actually represents the process itself (i.e. "the forces that shape the embryo").

It is widely believed that actomyosin contractility, in the form of apical constriction, drives gastrulation in anamniote organisms. Furthermore, histological evidence for apical constriction (showing "bottle-neck cells") has been presented previously for avian embryos, [73] so it is surprising to us that none of the current models for primitive streak formation, to our knowledge, explicitly involve or invoke actomyosin contractility. Our data suggest that the avian embryo, and more generally amniotes, utilize actomyosin contractility for epiblast morphogenesis, thus, perhaps, representing a more evolutionarily conserved mechanism than previously thought. We hope that our data spur further experimental and computational studies in this area to resolve the significant remaining challenges that exist in the field of gastrulation research.

Chapter IV

EFFECTS OF SUBSTRATE STIFFNESS ON PROSPECTIVE AVIAN CARDIAC CELL FATE

4.1 Introduction

4.1.1 Avian Cardiogenesis

In the avian pre-primitive streak blastula (EK stages X-XIV), [33] prospective heart cells occupy the posterior medial portion of the epiblast, the region of Kollers sickle from which the primitive streak extends [42] (Figure 7a).

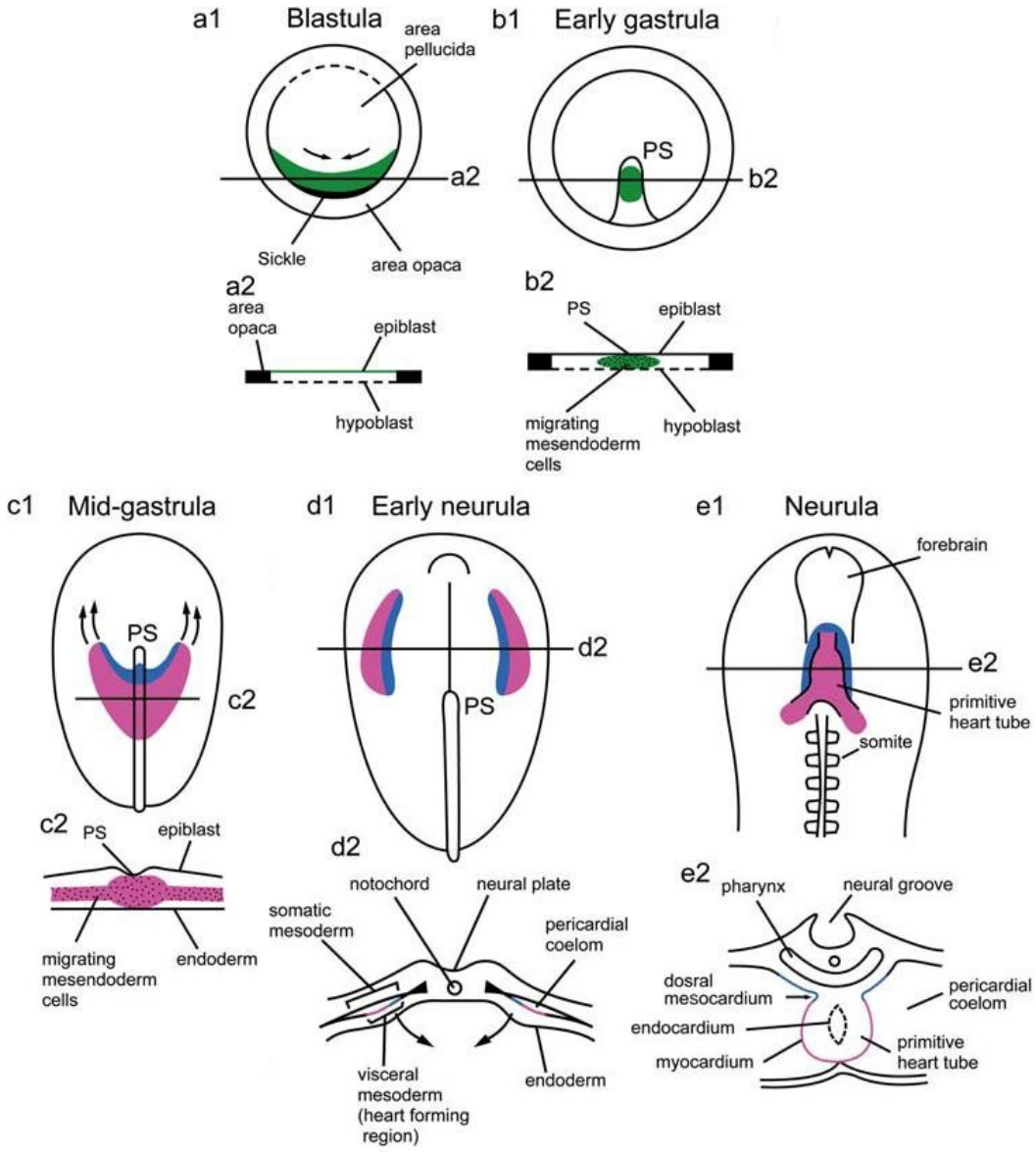

Figure 7: Fate mapping of avian cardiac progenitor cells (Nakajima et al. 2009).

After primitive streak formation during early stages of gastrulation (HH3), presumptive heart cells reside in the anterior half of the primitive streak (Figure 7b). By midprimitive-streak stages (HH4) (Figure 7c), cardiogenic cell ingression is complete, and somite-fated cells ingress in the same region. [35] The precursors of the 3 rostrocaudal divisions of the primitive heart tube also occur in that order within

the primitive streak, [81] [25] [94] though it has been shown that rostrocaudal patterning is not determined in the streak. [45] After ingression, cardiac regions migrate anterolaterally (HH5 and HH6) (Figure 7d) to form a lateral plate mesoderm on each side of the primitive streak, termed the precardiac mesoderm. [35] [90] [67] The most lateral portion of the lateral mesoderm are termed the heart forming regions (HFR). [19] These HFRs have been explanted and found to differentiate into heart muscle. [81] HFR cells are in continuous contact with the anterior endoderm. [92] At stage 6 cardiac precursors epithelialize, and during stage 7 they form the splanchnic (ventral) and somatic (dorsal) mesoderm separated by a space called the pericardial coelom [60] (pronounced see'-lum). N-cadherin localization has been shown to be essential during pericardial coelom formation and epithelialization of the differentiating myocardium. [60] The coelom cavities migrate and join at the ventral midline of the embryo and continue to fuse in the anterior and posterior directions [71] at the 4-somite stage in the quail embryo [27] and at the 7-somite stage in the chick embryo [94] to form the primitive heart tube (Figure 7e). Following these events, the heart tube loops and undergoes septation and valve formation.

4.1.2 SMAA in Heart Formation

Many markers have been shown to identify cardiac differentiation including N-cadherin [60] and myofibrillar proteins including troponin, [34] cardiac C-protein, [34] myosin heavy-chain, [34] myosin light-chain, tropomyosin, actin isoforms, [98] muscle $\alpha-$actinin, [30] and cNkx-2.5. [90] SMAA expression first marks the onset of cardiac cell differentiation [85] and SMAA is the major isoform of the actin family in vascular tissue. [98] [19] SMAA mRNA was first discovered during the early stages of heart tube formation in stages HH8 and HH9 avian cardiac tissue. [85] The earliest detection of SMAA transcripts in the embryo is stage HH5 in right and left anterior regions and is present in the coelom. [19] Translated SMAA was first seen at stage HH9, detected

exclusively in the heart. [98] It is first transcribed at HH7+, at the fusion of the bilateral heart forming regions. [19] At HH12, the smooth muscle alpha-actin was down-regulated in the heart, remaining only in the conus, which forms the vascular trunks [85] and SMAA is replaced by sarcomeric actin. [98]

4.1.3 Induction of Cardiac Myogenesis

4.1.3.1 Pregastrula Hypoblast

There are several signals necessary for proper cardiogenesis. Two known critical tissue interactions are necessary for myocardial cell specification. The first essential tissue interaction is between the pregastrula hypoblast and posterior epiblast during stages EK XI XIV. [97] [114] [55] [68] [67] At these stages, cardiac progenitor cells lie in the posterior region of the embryo in Kollers sickle. [42] It has been shown that the hypoblast can induce cardiac myocytes in anterior and posterior pre- and mid-gastrula epiblast (stage HH1, HH3) and can induce a limited amount of cardiac cells in stage 4 posterior primitive streak, suggesting that signaling from the hypoblast prior to stage 3 is required for cardiac myogenesis. [114] There are many potential inducing factors in the pregastrula hypoblast. Activin, TGFβ-1, and FGF-4 (but not BMP-2 or -4) can induce cardiac myogenesis in the stage EK XI XIII posterior epiblast, [55] where the cardiac progenitor cells reside at that stage. Activin has been shown to induce a notochord and somites in stage XIII epiblast. [69] In addition, explants from the epiblast or posterior PS have shown a dose−dependent response to activin resulting in a number of mesodermal cell types, suggesting that activin may play a role in multiple signaling pathways at various embryo stages. [97] Cardiac myocytes can be induced from the posterior epiblast with activin, and inhibited by the activin-binding protein follistatin. [114] [24] Fgf8b is expressed in the hypoblast, and an anti-FGF8b antibody inhibits the expression of BMP-independent cardiomyocyte genes such as SMAA, cTNT, and Tbx5. [67]

4.1.3.2 Anterior Lateral Endoderm

The second cardiac-inducing tissue interaction occurs between the heart forming regions of the anterior lateral mesoderm and the anterior lateral endoderm at stage HH5. [6] [99] [90] [91] [55] [75] The anterior lateral endoderm from stage HH5 did not effectively induce cardiogenesis in epiblast cells, but was able to induce cardiac myocytes in stage 4 primitive streak cells. [114] In the anterior lateral endoderm, fibroblast growth factor 2 (FGF-2), [100] activin-A, [99] and IGF-II [7] play a role in cardiac induction. Anterior lateral endoderm produces BMP-2 and FGF-4, which in combination can induce cardiac myogenesis in stage 5/6 posterior mesoderm. [62] However, BMP-2 and -4 cannot induce cardiac myocytes in stages EK XI XIV, [55] which suggests that BMP signaling occurs after these stages. Activin is produced in the anterior lateral endoderm and supports cardiac differentiation in the posterior mesoderm. [99] Schultheis [90] did inductive experiments on the posterior primitive streak of stage 4 embryos in which he showed that these normally non-cardiogenic cells can be induced to become cardiac myocytes with anterior lateral endoderm or anterior central mesoderm. His hypothesis suggests that signaling molecules in the anterior endoderm can induce cardiac myogenesis while inductive and inhibitory signals act in the anterior mesendoderm.

There are a few possible explanations for cardiac induction. Cardiac myocytes could be induced by the hypoblast at stage 2-3 and then maintained by the AL endoderm. Both signals from the hypoblast and endoderm could be required to act simultaneously. The signaling could be initiated by the hypoblast and then specified by the endoderm. It is not either-or, because epiblast cannot be induced with endoderm signals, [55] [114] so it seems that hypoblast signaling precedes endoderm signaling in the process.

Yatskievych [114] asserts that myocardial cell specification is underway by stage 3, as explants from stage 3 can form cardiac myocytes. Inagaki [45] did explant studies

that showed that regions of the PS normally destined to form the heart do not do so when transplanted to other regions of the streak. The differences between these 2 scenarios is the in the Yatskievych scenario, tissues were explanted and therefore not subjected to further signaling in the embryo, whereas in the Inagaki experiments, explants were transplanted and subjected to further signaling within the embryo. This suggests that inhibitory signaling plays a role in the embryo to specify fated heart cells.

There have been many developmental cardiac differentiation studies using embryonic explants from gastrula and pre-gastrula avian embryos (stage HH1-3, 0-12 h of incubation) over the past twenty years, but most of these have been conducted on glass [67] [68] [55] [114] [30] [99] [6] [37] or a collagen gel [91] or a floating filter raft. [90] Differentiated embryonic cardiac myocytes (harvested at 4, 7, and 10 days of incubation) have previously been cultured on flexible substrates to assess an ideal substrate stiffness for beating, [31] and 3-day-old (after heart formation and looping) embryonic cardiac myocytes have been cultured on soft substrates to assess cardiac differentiation, [115] but no rigorous study has been completed to examine the role of mechanics − specifically, substrate stiffness − in early heart development reminscent of the body of previous work on gastrula and pre-gastrula embryos (0-12 h incubation and prior to heart formation). The objective of this study is to determine the effects of substrate stiffness on cardiac induction. An initial immunofluorescence screening of cardiac markers including sarcomeric $\alpha-$actinin, smooth muscle alpha actin (SMAA), E-cadherin, N-cadherin, MF20, $\beta 1$ integrin, vinculin, and Nkx2.5 yielded positive staining for SMAA, E-cadherin, and vinculin. Explants from the anterior and posterior primitive streak of quail embryos were cultured on fibronectin-coated 70 kPa and 250 kPa Sylgard 527 PDMS (Figure 8). Samples were stained with E-cadherin, SMAA, and Vinculin, the the same field was imaged for all 3 stains. Images were exported to Matlab for quantitative analysis. The staining of these three markers has

been quantified to show that substrate stiffness alters the differentiation of precardiac cells, as indicated by SMAA, E-cadherin, and vinculin staining patterns.

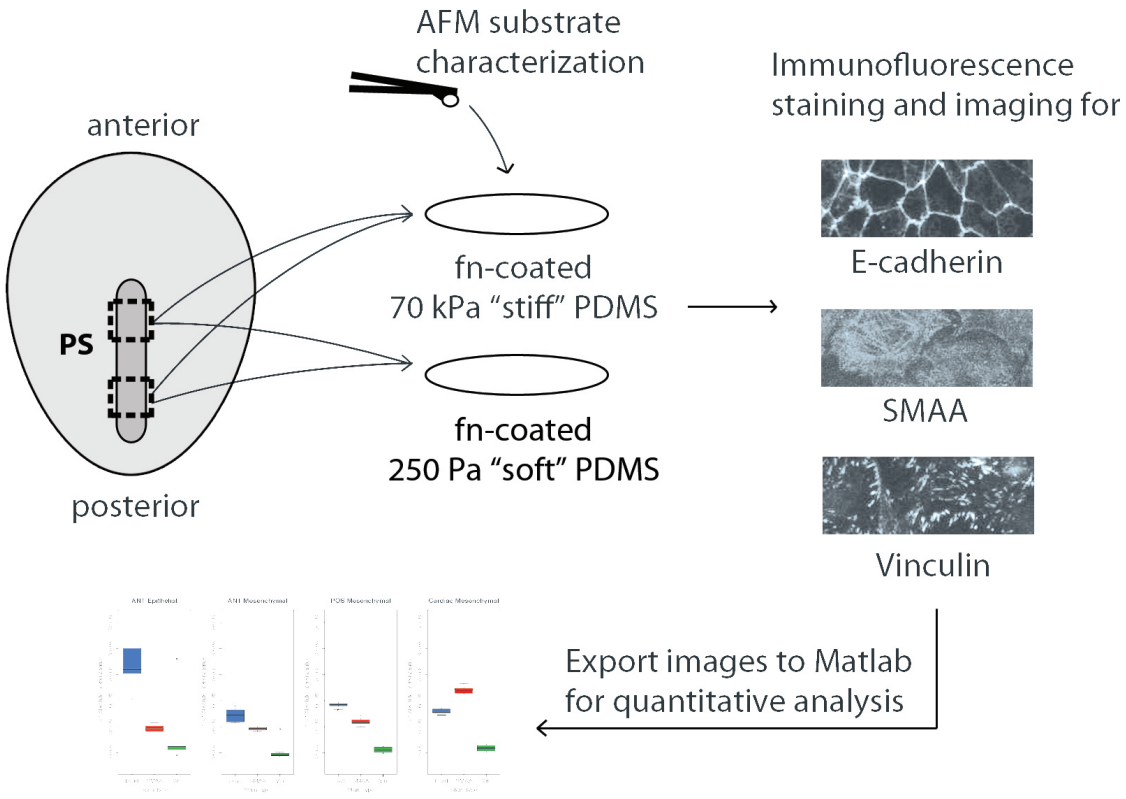

Figure 8: Experimental overview

Explants from the anterior and posterior primitive streak were cultured on fibronectin-coated 70 kPa and 250 kPa Sylgard 527 PDMS. Samples were stained with E-cadherin, SMAA, and Vinculin, the the same field was imaged for all 3 stains. Images were exported to Matlab for quantitative analysis.

4.2 Methods and Materials

4.2.1 PDMS fabrication

Dow Corning SYLGARD® 527 A/B Silicone (polydimethysiloxane) Dielectric Gel was combined in ratios of 0.1:1 and 1.5:1 (A:B) (wt%) and mixed vigorously with a pipette tip for 5 minutes. 50 μL of the mixture was pipetted onto 18-mm glass

coverslips in a Laurell Spin Coater (WS-400BZ-6NPP) and spun at 1500 rpm for 10 seconds. 0.1:1 coverslips were cured in a silanized dish at 90 °C for 24 h and 25 °C for 24 h. 1.5:1 coverslips were cured at 70 °C for 72 h and 25 °C for 24 h. In particular for the "soft" PDMS, cure time was empirically determined by placing a clean coverslip on top of the cured PDMS layer on its coverslip. Substrates were considered "cured" if the clean coverslip could be pulled away without disturbing the surface features and continuity of the PDMS substrate and with no reside remaining on the clean coverslip.

4.2.2 Atomic force microscopy

An MFP-3D atomic force microscope from Asylum Research (Santa Barbara, CA) (setup described previously, [44]) was used to characterize the stiffness of the SYLGARD® 527 substrates in ratios of 0.1:1 and 1.5:1 (A:B). To decrease surface tension and simplify contact mechanics, a 15$-\mu$m-diameter polystyrene bead was attached to a Bruker triangular AFM cantilever (Figure 9a). Indentation force curves (force vs. indentation) were fitted to the Hertz model to determine the modulus for 0.1:1 PDMS indentations (described previously [44]). However, we found that the modulus varied with indentation depth for the "soft" 1.5:1 PDMS substrates. Therefore, using the Hertz model, we plotted the modulus vs. indentation depth for each indentation in 1.5:1 PDMS and averaged the moduli in the linear region of the curve (sample curve, Figure 9b). Measurements were taken under water at room temperature in a 50-mm fluorodish from World Precision Instruments (Sarasota, FL). Three regions per sample were indented with 5 indentations per region across several sample preparations.

4.2.3 Fibronectin-substrate coating

PDMS substrates were coated with fibronectin (FN) as follows. PDMS-coated 18-mm coverslips were incubated with 10μg/mL FN overnight at 37 °C and washed 3 times with sterile PBS.

4.2.4 Anterior and posterior primitive streak culture

Embryos were cultured at stage HH3 (12 14 h) using the New egg culture technique. [74] Anterior and posterior primitive streak explants were cut using sterile glass needles pulled with a micropipette puller (Narishige Model PC-10) under a dissecting microscope (Leica MZ16F). Explants were placed on FN-coated PDMS substrates in serum-free media (RPMI 1640 + 1% ITS + 1% P/S) and incubated at 37 °C for 72 h.

4.2.5 Cardiac cell isolation

Hearts were harvested from 3-day-old quail embryos using sterile glass needles pulled with a micropipette puller (Narishige Model PC-10). After incubating in 1x (0.05%) trypsin + 0.5 mM EDTA at 37 °C for 15 minutes and quenching with media (DMEM-F12 + 10% FBS + 1% P/S), the tissue was gently dissociated by 50 passes in a 2 mL pipette tube. Cells were pelleted at 500 rpm for 5 minutes, resuspended in fresh media, and seeded at a density of 6 hearts per 18-mm substrate in a 12-well plate and incubated at 37 °C for 72 h.

4.2.6 Immunofluorescence staining and imaging

Primitive streak and cardiac cell cultures were rinsed with ice-cold PBS, incubated in ice-cold Cytoskeleton (CSK) Buffer [10 mM PIPES buffer, 50 mM NaCl, 150 mM sucrose, 3mM $MgCl_2$, 1 mM PMSF, 1 g/mL leupeptin, 1 g/mL aprotinin, 1 g/mL pepstatin] for 2 minutes, incubated in 2 separate washes of CSK buffer with 0.5% (v/v) Triton X-100, and fixed for 30 minutes in 3% paraformaldehyde in PBS at 25 °C. Samples were washed 3 times with DPBS and blocked with 3% BSA in PBS + 0.05% sodium azide (blocking buffer) for 1 h at 25 °C. Samples were then incubated with a primary vinculin antibody (SIGMA V4505, clone VIN-11-5) at a concentration of 2.6 mg/mL diluted in blocking buffer for 1 h at 25 °C, rinsed 3 times with DPBS for 5 minutes each, incubated with Alexa Fluor® 488-conjugated goat

anti-mouse isotype-IgG1-specific secondary (Jackson ImmunoResearch 115-545-205) at 14 μg/mL, and rinsed 3 times with DPBS for 5 minutes each. Smooth muscle alpha actin (SMAA) monoclonal antibody (Pierce MA1-06110, isotype IgG2a, clone 1A4) was directly conjugated to rhodamine phalloidin using an EasyLink Rhodamine Conjugation Kit (Abcam ab102915). Samples were incubated with the SMAA direct conjugate (1 g/mL) and Alexa Fluor® 647 Mouse anti-E-Cadherin direct conjugate (BD Pharmingen 560062, isotype IgG2a) at 5 μg/mL for 1 h at 25 °C, then rinsed 2 times with DPBS and once with Millipore water for 5 minutes each. Samples from each experimental group were labeled with isotype controls at the same concentration as the corresponding primary antibody for 1 h at 25 °C (Alexa Fluor® 647 Mouse IgG2a Isotype Control, BioLegend 400234; DylightTM 488 conjugate IgG1 Isotype Control, Enzo Life Sciences ADI-SAB-600-488; Rhodamine conjugated Mouse IgG2a Isotype Control, Rockland 010-0041), then rinsed 2 times with DPBS and once with Millipore water for 5 minutes each. Samples were mounted ProLong® Gold Antifade Reagent. Images were taken on a Leica DMI6000B inverted microscope with a Ludl Mac5000 controller and Hamamatsu ORCA-ER camera at 10x with 1x1 binning. Exposure time was set using isotype controls before imaging each experimental group. The 10x magnification and 1x1 binning were selected by imaging several samples at 5x, 10x, and 20x and at 1x1 and 2x2 binning, importing the images into Matlab, and quantifying per usual with absolute and ratio intensities. The 10x magnification and 1x1 binning were selected based on the quantification results—staining differences were best captured (differences within the same regions showed the most differences) under these conditions.

4.2.7 Image analysis

Images were imported into MATLAB for calculating absolute values and ratios of immunoflourescence staining for each marker.

4.2.8 Statistical analysis

Statistical analyses were performed in R (`http://www.r-project.org`), a free software environment for statistical computing and graphics, and paired t tests were conducted in Numbers from the iWork suite.

4.3 Results

4.3.1 Substrate mechanical characterization

The substrate used in this study, polydimethylsiloxane (PDMS) (Dow Corning SYLGARD® 527 A/B Silicone Dielectric Gel) was chosen for its range of moduli in addition to its biological inertness and optical translucence. Coverslips were spin-coated (see Methods) and cured, then tested on a MFP-3D atomic force microscope. PDMS ratios of 0.1:1 (A:B) and 1.5:1 were mixed in multiple preparations, then indented 5 times in different regions. Data were shown to be consistent through multiple substrate preparations.

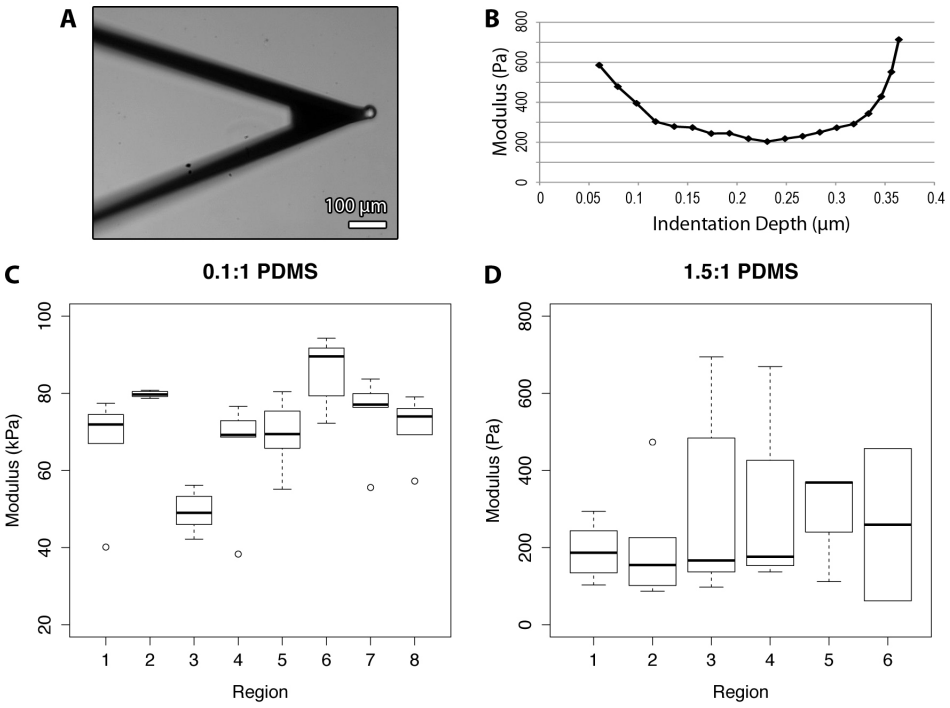

E

0.1:1 (A:B) PDMS	
Region	**Modulus (kPa)**
1	66.2 ± 15.1
2	79.8 ± 0.9
3	49.3 ± 5.6
4	65.1 ± 15.3
5	69.2 ± 9.7
6	85.4 ± 9.3
7	74.5 ± 11.0
8	71.1 ± 8.5

F

1.5:1 (A:B) PDMS	
Region	**Moduli (Pa)**
1	191.4 ± 75.0
2	199.6 ± 143.6
3	315.8 ± 261.6
4	289.7 ± 253.9
5	283.8 ± 149.0
6	259.4 ± 279.4

Figure 9: AFM characterization of PDMS substrates

A) Bruker triangular AFM cantilevers were funtionalized for this study by attaching a 15−μm-diameter polystyrene bead. B) Sample of a modulus (E) vs. indentation plot used to determine the moduli of indentations on "soft" 1.5:1 PDMS. C) Moduli of regions of 0.1:1 PDMS. Boxes represent the 25th to 75th percentiles, and the heavy line represents the median. Whiskers represent the top and bottom quartiles of the data. Outliers (less than or greater than 1.5 times the inner quartile range) are denoted by open circles. D) Moduli of regions of 1.5:1 PDMS. E) Modulus per region with standard deviations for 0.1:1 PDMS. F) Modulus per region with standard deviations for 1.5:1 PDMS.

A Bruker triangular AFM cantilever was functionalized for indenting PDMS by attaching a 15$-\mu$m-diameter polystyrene bead to the tip (Figure 9a). Indentations were fit to the Hertz model for 0.1:1 "stiff" PDMS indentations, however, we found that there was often not a straightforward fit to the Hertz model for force curves of the 1.5:1 PDMS "soft" substrates. Therefore, using the Hertz model, we plotted the modulus vs. indentation depth for each indentation in 1.5:1 PDMS and averaged the moduli in the linear region of the curve (Figure 9b). We show the measured moduli per region of each PDMS ratio in plots (Figure 9c,d) and tables (Figure 9e,f). Interestingly, the variation across the regions shows the heterogeneity of the sample. Soft substrates are often characterized without a mention of possible variation within the microscturcture and modulus of the material. The average moduli of 250 Pa for 1.5:1 PDMS and 70 kPa for the 0.1:1 PDMS will be referred to throughout the remainder of this paper as "soft" and "stiff" for simplicity.

4.3.2 SMAA, ECad, and VIN image quantification distinguishes between cell types

The heterogeneity of primitive streak explants and regional differences in markers and morphology prompted us to devise an unbiased imaging method to quantify differences between marker expression in different regions. After a cardiac marker screening for smooth muscle alpha actin, sarcomeric $\alpha-$actinin, E-cadherin, N-cadherin, vinculin, MF20, β1 integrin, and Nkx2.5, we found that the strongest markers for the primitive streak explants were smooth muscle alpha actin (SMAA), E-cadherin (ECad), and vinculin (VIN). After setting exposure time according to isotype controls (see Methods), we took images of 4 specific cell/morphology types. First, the anterior primitive streak explants exhibited both epithelial and mesenchymal regions, and both were imaged. Second, the posterior primitive streak exhibited primarily mesenchymal cell regions. Lastly, cultured cardiac cells isolated from 3-day-old beating embryonic hearts (see Methods) displayed purely mesenchymal fields. The same

field was imaged for each of the three markers (SMAA, ECad, VIN) for each sample in each of the 4 cell types. The results of our primary experiment on glass can be seen in Figure 10.

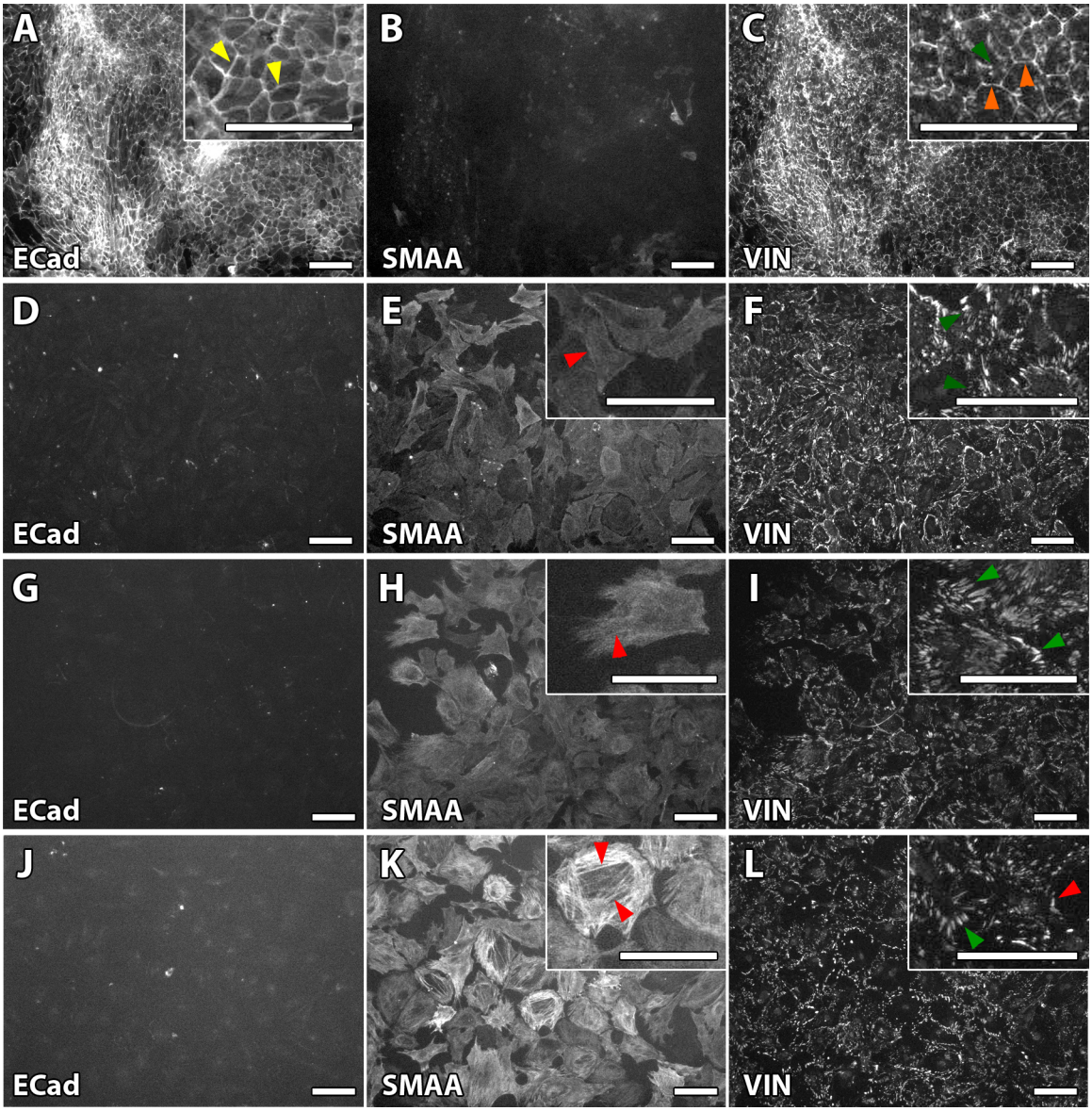

Figure 10: Anterior and posterior primitive streak explants and cardiac cells on glass. Rows represent the same field of a sample image from each of 4 experimental groups: epithelial cells from the anterior primitive streak (A,B,C), mesenchymal cells from the anterior primitive streak (D,E,F), mesenchymal cells from the posterior primitive streak (G,H,I), and mesenchymal cardiac cells (J,K,L). Columns represent each marker: E-Cadherin (A,D,G,J), SMAA (B,E,H,K), and Vinculin (C,F,I,L). ALL SCALE BARS ARE 100 μm.

The epithelial region of anterior primitive streak explants on FN-coated glass (first row, Figure 10a,b,c) exhibited E-Cadherin staining at the cell-cell borders (yellow arrowheads, in Figure 10a inset). Cells appear to form a single layer of cuboidal epithelial cells. There were low levels of SMAA staining (Figure 10b) with 2 or 3 cells in the field expressing SMAA. This was not surprising considering that precardiac cells do not re-epithelialize until stage HH6 when they form the splanchnic (ventral) and somatic (dorsal) mesoderm (Figure 7d2) and SMAA translation does not occur until stage HH9. Vinculin appears at the cell-cell junctions and is colocalized with E-Cadherin at the cell boarders (orange arrowheads, Figure 10c inset). In addition, vinculin is localized to focal adhesions beneath the epithelial cells (green arrowheads, Figure 10c inset). The pattern of focal adhesions is just inside the cell periphery, and they are largely not present at the cell centers.

In the mesenchymal region of anterior primitive streak explants on FN-coated glass (second row, Figure 10), there was little to no E-caderin staining, which is not surprising given the mesenchymal phenotype. Any glimpse of E-cadherin was not localized to the cell borders. The mesenchymal region of the anterior primitive streak exhibited SMAA staining, which was interesting because, as we have stated previously, this is the specific region where precardiac cells reside, and SMAA is the first cardiac marker. While SMAA appears to be ubiquitous throughout the cells, it is also localized to filaments that span the cell (red arrowhead, Figure 10e inset) and if there is any heterogeneity in the expression, SMAA tends to be localized in filaments more to the peripheries than the center of the cells. In the mesenchymal anterior primitive streak, vinculin was visible in focal adhesions throughout the cell but in particular heavily dotting the cell borders (green arrowheads, Figure 10f inset).

The posterior primitive streak on FN-coated glass (third row of Figure 10) exhibited a predominantly mesenchymal phenotype without any epithelial regions. Similar to the mesenchymal region of the anterior primitive streak, there was no E-cadherin

staining (Figure 10g). SMAA staining was seen throughout the cell and highlighted filaments spanning the cells that generally ran closer to the cell periphery than center (red arrowhead Figure 10h inset). A difference between the anterior and posterior primitive streak mesenchymal regions was the cell spreading. Across all images, the posterior primitive streak showed cells more spread than the anterior region. Vinculin staining was localized to often elongated focal adhesions (green arrowheads, Figure 10i inset) at the cell periphery and more compact focal adhesions throughout the rest of the cell area.

Cardiac cells on glass (bottom row, Figure 10) were largely negative for E-cadherin, and any visible fluorescence was not localized to the cell border. SMAA staining showed very distinct and concentrated actin filaments (red arrowheads, Figure 10k inset) and overall staining was the brightest of the four cell types. Cell spreading was comparable or larger than mesenchymal posterior primitive streak cells. Vinculin was localized to focal adhesions throughout the cells but concentrated at the cell borders (green arrowheads, Figure 10l inset).

Of the 4 cell types, only the epithelial anterior primitive streak cells were positive for E-cadherin (column 1 of Figure 10). All 3 mesemchymal phenotypes were positive for SMAA (column 2 of Figure 10) with the cardiac cells exhibiting the highest level of staining (quantified in Figure 9). Lastly, vinculin was positive in all 4 cell types (column 3 of Figure 10), but while it was localized to focal adhesions in all 4 cell types, it was only localized to cell-cell junctions in the epithelial anterior primitive streak cells.

To strengthen the comparisons between differences in the intensities of the stains in different regions and to address the heterogeneity of the samples and the similar phenotypes of the mesenchymal cells from different regions, we developed an unbiased method to quantify differences between regions. We imported the raw images into Matlab and plotted the fluorescence intensities for each stain across all samples from

each sample type (Figure 11a-d). We noticed that across all repetitions of these experiments the intensity of vinculin staining appeared to be at a similar level for all sample groups and provided a "baseline" stain across all groups regardless of region or substrate. In an effort to take into account field-to-field differences between the 10x images (i.e., cell spreading, sample morphology, and cell count), we normalized the E-cadherin and SMAA intensities to the vinculin fluorescence intensity (E/V and S/V) for each sample (Figure 11e-h) to express the E-cadherin and SMAA staining levels while accounting for differences between fields. We believe this is the most accurate method, that is, showing the actual differences between the sample types and the clearest method for the purpose of comparison.

It is important to note that the representative images shown in this study have been optimized to display cell features of interest, however, *all quantification has been conducted on raw images* using tif files taken directly from the microscope.

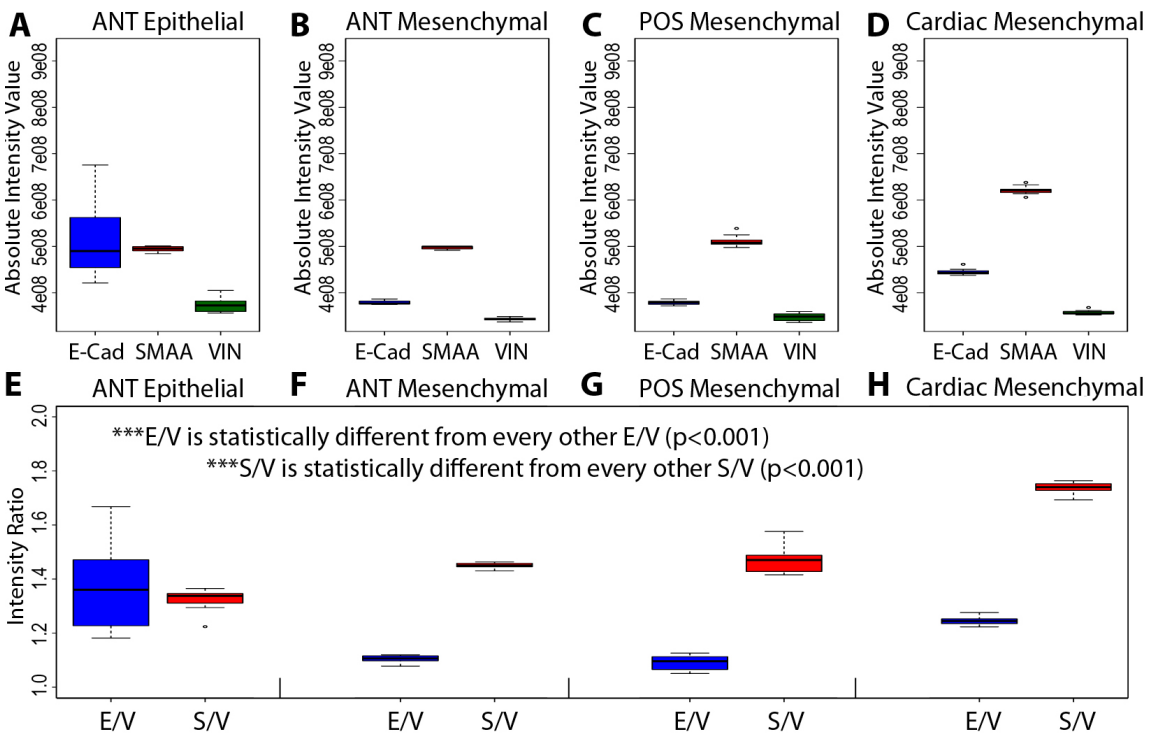

Figure 11: Ecad, SMAA, and VIN intensity in anterior and posterior primitive streak explants and cardiac cells on glass.

The boxes represent the 25th to 75th percentiles, and the heavy line represents the median. Whiskers represent the top and bottom quartiles of the data. Outliers (less than or greater than 1.5 times the inner quartile range) are denoted by open circles. The absolute intensity value of each marker is displayed for anterior PS explants epithelial cells (A), anterior PS explant mesenchymal cells (B), posterior PS explant mesenchymal cells (C), and mesenchymal cardiac cells (D). ECad and SMAA levels are normalized to the vinculin staining for each cell type directly beneath (E,F,G,H).

On glass, the absolute intensities of E-cadherin reflect the observations of the previous figure. E-cadherin levels are highest in the epithelial anterior primitive streak explants (Figure 11a), lowest in the mesenchymal regions of the anterior and poster primitive streak explants (Figure 11b,c), and only slightly higher in the cardiac cells

(Figure 11d). SMAA levels escalate across the board. As previously discussed, we believe the ratios and not the absolute intensities give the most accurate quantification, taking into account the variables of cell count and spreading. The apparent closeness of the SMAA staining in epithelial (Figure 11a) and mesenchymal (Figure 11b) anterior primitive streak is the most apparent example. Posterior primitive streak absolute SMAA levels (Figure 11c) are slightly higher than the anterior primitive streak explants (Figure 11a,b), and the cardiac cells have the highest level of SMAA staining (Figure 11d). The vinculin staining levels were identical for all mesenchymal regions (Figure 11b,c,d), but were slightly elevated for the anterior epithelial group (Figure 11a). It is important to note that using this method, we do not consider it valuable to compare staining levels of different stains in the same sample because even though we use isotype controls (see Methods), we use different antibodies for each protein of interest. Each antibody has unique binding properties, which vary between our 3 markers of interest. Our intensity readings measure the comparative presence of each antibody under different experimental conditions, not the antigen itself. Our method quantifies the presence of an antibody as an indicator of its antigen, not a direct quantification of the antigen. In addition, the stains are imaged using different filters. Therefore, we would like to be clear that the primary comparison is same marker between different sample types or substrates and not between markers within the same sample. This method was devised to quantify regional differences within samples that would not be apparent using a method that would not distinguish between regions, such as flow cytometry or western blotting.

Once we "normalize" the E-cadherin and SMAA stains to vinculin (E/V and S/V), the trends are still more clear. E/V is highest in the anterior epithelial region (Figure 11e), lower in the mesenchymal region of the anterior primitive streak (Figure 11f), and lowest in the posterior primitive streak. Cardiac cells exibit a slightly higher E/V still below that of the epithelial anterior primitive streak explants (Figure 11h). E/V

comparisons between all groups are statistically significant ($p<0.001$). S/V steadily increases across the sample types. The mesenchymal region of the anterior primitive streak has a significantly higher S/V than the epithelial regions ($p<0.001$), and the mesenchymal posterior primitive streak has a higher S/V than the mesenchymal anterior primitive streak ($p<0.01$). As expected, the cardiac cells have the highest S/V ($p<0.001$).

Here we have shown that this method of quantification distinguishes between the different phenotypes seen under the miscroscope with statistical significance. As previously discussed, glass has been used for a majority of embryo explants cardiac differentiation studies, and so it is a good starting point before moving on to our primary comparison of interest, that of substrates of different stiffnesses. Because we will be using PDMS for our substrate stiffness study, we cannot directly compare the PDMS data to our data from explantation studies on glass due to differences in fibronectin adsorption to the two surfaces. It has been extensively shown and accepted that exposing cells to different concentrations of ECM components can vastly alter their behaviors. [9]

4.3.3 Cardiac marker SMAA decreases in presumptive cardiac cells on softer substrate

Explants from the anterior and posterior PS and cardiac cells were cultured on "soft" (250 Pa) and "stiff" (70 kPa) PDMS substrates coated in passively-adsorbed fibronectin. Overall, the localization of ECad, SMAA, and vinculin remained similar to our previous experiment (Figure 12, Figure 13); however, the image quantification (Figure 14) showed that precardiac cells in the anterior PS behave differently on "soft" and "stiff" PDMS.

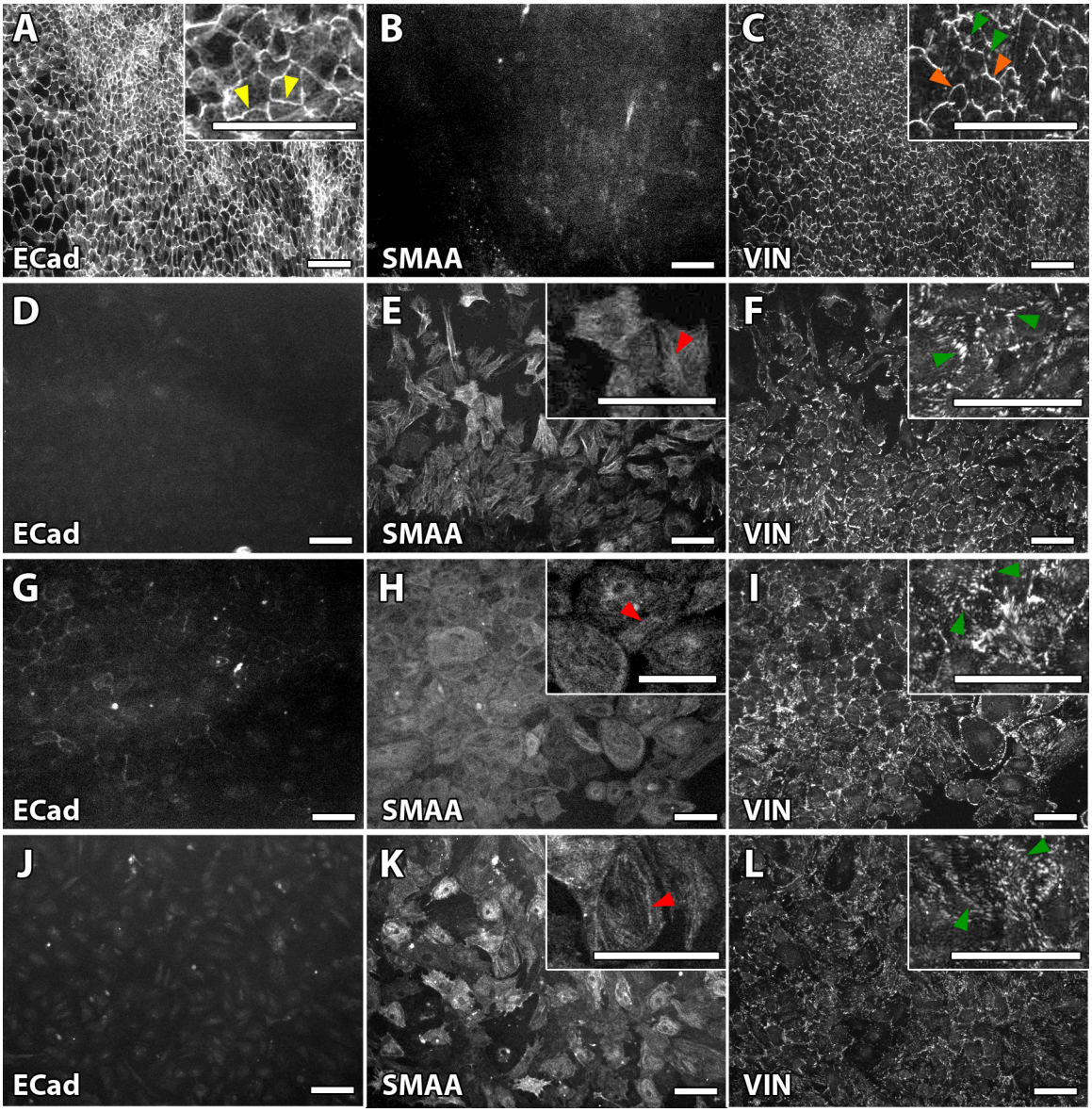

Figure 12: Anterior and posterior primitive streak explants and cardiac cells on "stiff" (70 kPa) PDMS. Rows represent the same field of a sample image from each of 4 experimental groups: epithelial cells from the anterior primitive streak (A,B,C), mesenchymal cells from the anterior primitive streak (D,E,F), mesenchymal cells from the posterior primitive streak (G,H,I), and mesenchymal cardiac cells (J,K,L). Columns represent each marker: E-Cadherin (A,D,G,J), SMAA (B,E,H,K), and Vinculin (C,F,I,L). ALL SCALE BARS ARE 100 μm.

On "stiff" FN-coated PDMS (70 kPa), the trends in morphology and staining appear to be similar to cultures on glass. In the epithelial region of anterior primitive streak explants (first row, Figure 12) E-cadherin and vinculin were co-localized in the cell-cell borders (yellow arrows, Figure 12a and orange arrows, Figure 12c). Vinculin was also localized to focal adhesions throughout the cells (green arrows Figure 12c). As expected, there were low levels of SMAA staining in the epithelial anterior primitive streak explants, and no distinct patterns of staining were visible (Figure 12b).

The mesenchymal region of the anterior primitive streak on glass (second row, Figure 12) showed low levels of E-cadherin staining with no discernible features (Figure 12d). SMAA was present in all mesenchymal anterior primitive streak cells (Figure 12e) and was localized to filaments across the cells (red arrowheads, Figure 12e inset). It appears that faint nucleus outlines are visible as darkened regions in the SMAA staining. Again, this cell type is of primary interest as we believe these cells to be cardiac precursors isolated from the streak. As with the mesenchymal anterior primitive streak explants on glass, this cell type on 70 kPa PDMS exhibited localization to focal adhesions throughout the cells (Figure 12f) but preferentially around the cell periphery (green arrowheads, Figure 12f inset).

In the mesenchymal posterior primitive streak region (third row, Figure 12), an interesting pattern was seen in some regions of E-cadherin staining. Faint E-cadherin staining was visible in the cell-cell borders (Figure 12g) of SMAA-expressing cells (Figure 12h). This phenomena was seen in a few places in approximately 33% (4 of 12) of the samples and not in all regions of SMAA-expressing cells. As with cultures on glass, the SMAA-expressing cells in posterior primitive streak explants were generally more spread than the anterior primitive streak cells and showed fibers spanning the cells (red arrowhead, Figure 12h inset). Vinculin was localized to focal adhesions throughout the cell (Figure 12i), particularly those at the cell edge (green arrowheads, Figure 12i inset).

Cardiac cells on 70 kPa PDMS (bottom row, Figure 12) showed low levels of E-cadherin staining, which was not present at cell borders (Figure 12j). SMAA levels appeared to be highest in cardiac cells of the four sample groups (Figure 12k). As previously, SMAA was localized to distinct fibers across the cells (red arrowhead, Figure 12k inset) and an absence from the nuclear region is visible. Also similarly to cultures on glass, cardiac cells expressed vinculin in focal adhesions throughout the cell (Figure 12l) and elongated focal adhesions at the cell borders (green arrowheads, Figure 12l inset).

Overall, of all the sample types, only the epithelial region of the anterior primitive streak explants had significant E-cadherin staining (first column, Figure 12), all of the mesenchymal regions expressed SMAA with the cardiac cells expressing the highest levels of SMAA (second column, Figure 12), and all samples expressed vinculin in focal adhesions, with the epithelial anterior primitive streak explants also expressing vinculin in the cell-cell junctions (third column, Figure 12).

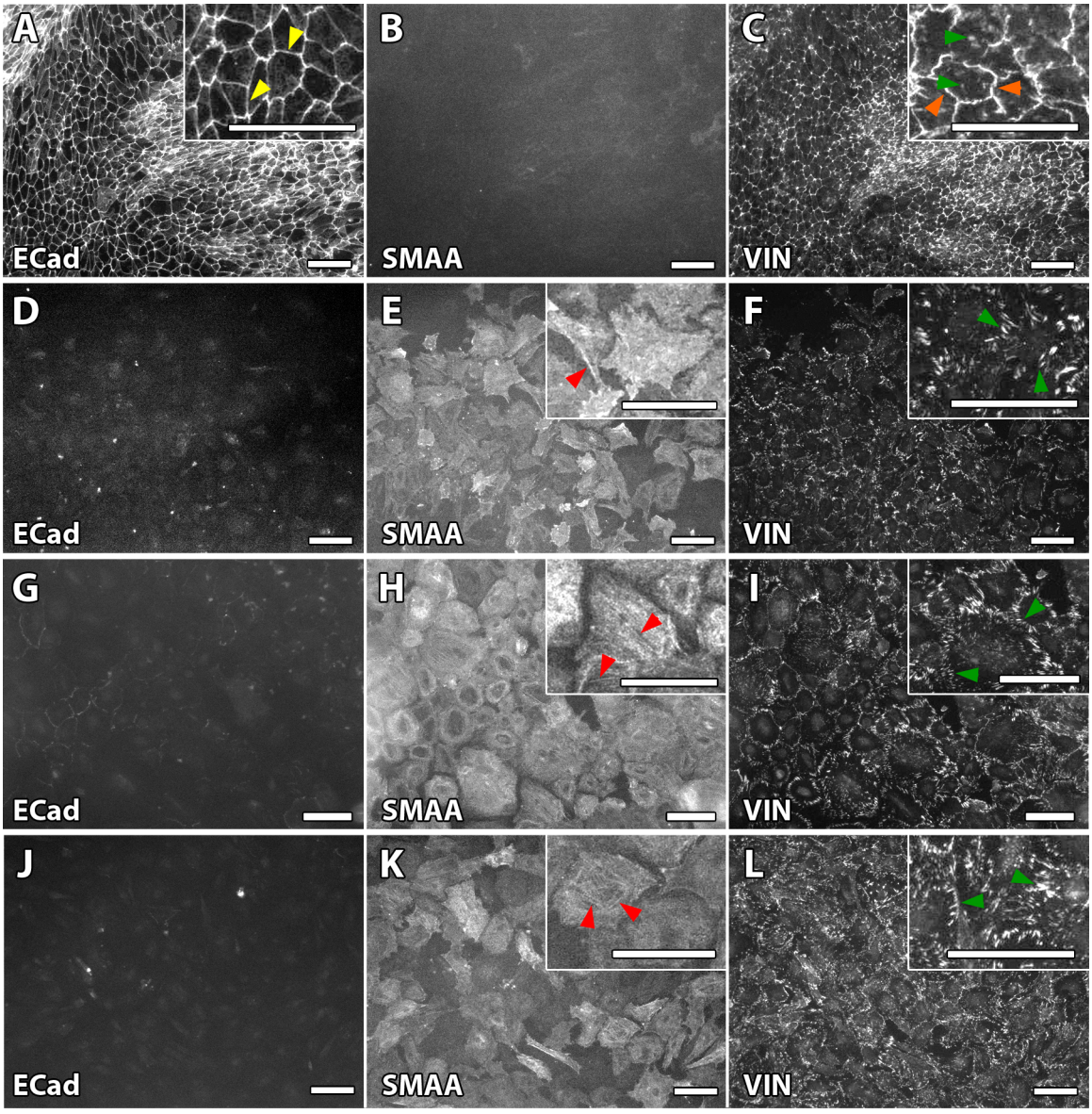

Figure 13: Anterior and posterior primitive streak explants and cardiac cells on "soft" (250 Pa) PDMS. Rows represent the same field of a sample image from each of 4 experimental groups: epithelial cells from the anterior primitive streak (A,B,C), mesenchymal cells from the anterior primitive streak (D,E,F), mesenchymal cells from the posterior primitive streak (G,H,I), and mesenchymal cardiac cells (J,K,L). Columns represent each marker: E-Cadherin (A,D,G,J), SMAA (B,E,H,K), and Vinculin (C,F,I,L). ALL SCALE BARS ARE 100 μm.

The cultures on "soft" 250 Pa FN-coated PDMS (Figure 13) show similar patterns to those of "stiff" 70 kPa PDMS, which highlights the necessity of our quantification method for meaningful comparisons between the two that will elucidate the connection between cardiac differentiation and substrate stiffness. In the epithelial anterior primitive streak explants (first row, Figure 13), E-cadherin and vinculin were co-localized to cell-cell junctions (yellow arrowheads, Figure 13a inset and orange arrowheads, Figure 13c inset, respectively), and there were low levels of SMAA staining with no discernible features (Figure 13b).

Mesenchymal regions of the anterior primitive streak (second row, figure 11), were negative for E-cadherin staining (Figure 13d). SMAA expression was localized to filaments across the cells (red arrowhead, Figure 13e inset), and vinculin staining was localized to focal adhesions, with a particular presence at the cell edges (green arrowheads, Figure 13f inset).

The mesenchymal posterior primitive streak on FN-coated 250 Pa PDMS (row 3, Figure 13) showed traces of E-cadherin at the cell-cell boundaries of SMAA-expressing cells, similar to the same cultures on 75 kPa PDMS (Figure 13g). SMAA-expressing cells (Figure 13h) were generally more spread than that anterior mesenchymal cells, and SMAA was localized to actin filaments (red arrowheads, Figure 13h inset) often traversing the non-central periphery of the cells. Vinculin staining was seen in focal adhesions concentrated at the cell edges (green arrowheads, Figure 13i inset).

Cardiac cells on FN-coated 250 Pa PDMS (bottom row, Figure 13) exhibited low levels of E-cadherin staining (Figure 13j) but the highest levels of SMAA staining across the sample groups on "soft" PDMS. SMAA was localized to filaments throughout the cell (red arrowheads, Figure 13k inset). Vinsulin was visible in elongated focal adhesions at the cell edges (green arrowheads, Figure 13l inset) and in focal adhesions throughout the cell.

In summary, E-cadherin staining on "soft" PDMS (column 1, Figure 13) was

mainly present in the epithelial anterior primitive streak cells and was barely visible in the cell-cell borders of some posterior primitive streak SMAA-expressing cells and in low level staining in the mesenchymal anterior primitive streak cells and cardiac cells. SMAA staining (column 2, Figure 13) was mainly expressed in the mesenchymal phenotypes, but also present in low levels of the epithelial anterior primitive streak cells. Vinculin expression (third column, Figure 13) was present in focal adhesions for all sample types throughout the cell and concentrated at the periphery for the mesenchymal phenotypes. It was co-localized with E-cadherin in the epithelial anterior primitive streak cells.

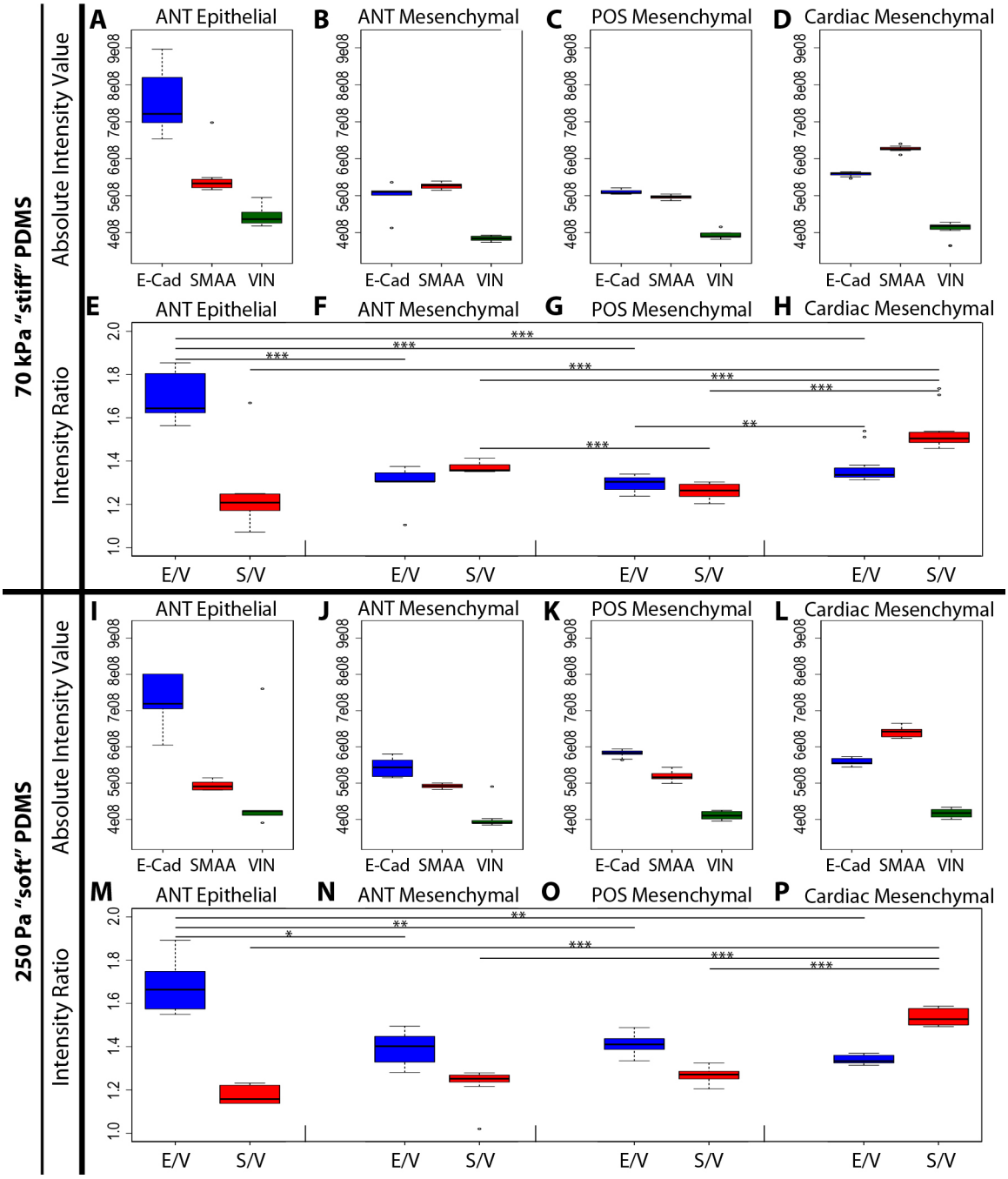

Figure 14: Caption next page.

Figure 14: (Previous page.) Ecad, SMAA, and VIN intensity in anterior and posterior primitive streak explants and cardiac cells on "stiff" (70 kPa) and "soft" (250 Pa) PDMS.

The boxes represent the 25th to 75th percentiles, and the heavy line represents the median. Whiskers represent the top and bottom quartiles of the data. Outliers (less than or greater than 1.5 times the inner quartile range) are denoted by open circles. The absolute intensity value of each marker is displayed for anterior PS explants epithelial cells (A), anterior PS explant mesenchymal cells (B), posterior PS explant mesenchymal cells (C), and mesenchymal cardiac cells (D). ECad and SMAA levels are normalized to the vinculin staining for each cell type directly beneath (E,F,G,H).

Figure 14 shows all quantified staining for cultures on "stiff" (70 kPa) (Figure 14a−h) and "soft" (250 Pa) (Figure 14i−p) PDMS, which reflect the staining patterns seen in Figure 12 and Figure 13. As previously stated, the raw intensity values (Figure 14a−d, i−l) do not account for field-to-field differences between the captured 10x sections for each image such as cell density and cell spreading, so we "normalized" the E-cadherin and SMAA intensity levels to the vinculin intensity for each image (E/V and S/V) and plotted these ratios (Figure 14e−h, m−p) in addition to the raw intensities. While we feel it is important for clarity to show the raw intensity data above the ratio data for each figure, we have seen that the ratio data gives a more "real" approximation of the actual staining patterns in the four sample groups, that is, the ratios correspond more closely to the staining seen under the microscope. To focus on the ratio data, we will parse out the comparisons for each sample type on "soft" and "stiff" PDMS in the following side-by-side figures (Figure 15, Figure 16, Figure 17, Figure 18). Still, within Figure 14, we can see comparisons between sample groups on the same substrate stiffness before moving on to look at the differences in our main variable: the effect of substrate stiffness on each sample type.

On "stiff" PDMS (Figure 14e-h), as expected the E/V of the epithelial anterior primitive streak cells (Figure 14e) was significantly higher ($p<0.001$) than all other sample groups. There were no further significant differences in E/V between sample types apart from the posterior primitive streak E/V (Figure 14g) being lower than the cardiac cell E/V ($p<0.01$) (Figure 14h). Cardiac cell S/V (Figure 14h) was significantly higher ($p<0.001$) than every other sample type. In addition, the mesenchymal anterior primitive streak cells (Figure 14f) had a significantly higher S/V than the mesenchymal posterior primitive streak explants (Figure 14g) ($p<0.001$), and no further comparisons of S/V yielded significant differences.

On "soft" PDMS (Figure 14m-p), E/V was again highest in the epithelial anterior primitive streak explants (Figure 14m) ($p<0.05$ compared to the mesenchymal region of the anterior primitive streak and $p<0.01$ for other regions). Unlike the results on "stiff" PDMS, where the cardiac E/V was significantly higher than the posterior primitive streak, on "soft" PDMS the posterior primitive streak E/V (Figure 14o) was significantly higher than that of the cardiac cells (Figure 14p)($p<0.001$). Cardiac cells showed the highest S/V (Figure 14p) ($p<0.001$ compared to other sample types), and there were no other statistically significant comparisons of S/V on "soft" PDMS.

Three interesting differences result from the collective cell type behaviors on "soft" and "stiff" PDMS. 1) Although S/V in the mesenchymal anterior primitive streak region is significantly higher than the posterior primitive streak on "stiff" PDMS ($p<0.001$), there is no statistical difference on "soft" PDMS, suggesting that the same level of SMAA staining was not reached in anterior primitive streak cells on the softer substrate relative to the posterior primitive streak cells. This is significant because the anterior primitive streak is where the precardiac cells reside, and the differentiation of these cells are the focus of this study. 2) On "stiff" PDMS, E/V for the cardiac cells was significantly higher ($p<0.01$) than that of the posterior primitive streak cells. Then on "soft" PDMS, the posterior primitive streak cells had a significantly

higher E/V, which suggests that the feint E-cadherin staining between some SMAA-expressing cells may have been more prevalent on the softer substrate. Finally 3) the statistical difference between the epithelial anterior primitive streak E/V and that of the rest of the sample types was less statistically significant on the softer substrate, further suggesting that the softer substrate influenced E-cadherin expression in these embryonic cells.

The next figures show comparisons of the same sample type on different substrates following the previous comparisons of different sample types on the same substrate.

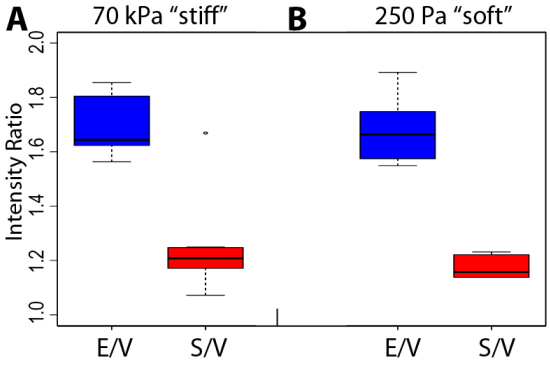

Figure 15: Side-by-side comparison of Ecad/VIN and SMAA/VIN intensity ratios for the epithelial region of anterior primitive streak explants on A) "stiff" (70 kPa) and B) "soft" (250 Pa) PDMS.

First, we compare the epithelial region of the anterior primitive streak cultures (Figure 15). As seen in the previous figures, E-cadherin staining was significantly ($p<0.001$) higher in this region than the others, which is reflected in the E/V ratio. However, there is no statistical difference in the E/V values between "stiff" (Figure 15a) and "soft" (Figure 15b) PDMS, nor is there any difference in the S/V ratio. We can conclude that the substrate stiffness did not affect the epithelial region of the anterior primitive streak explants.

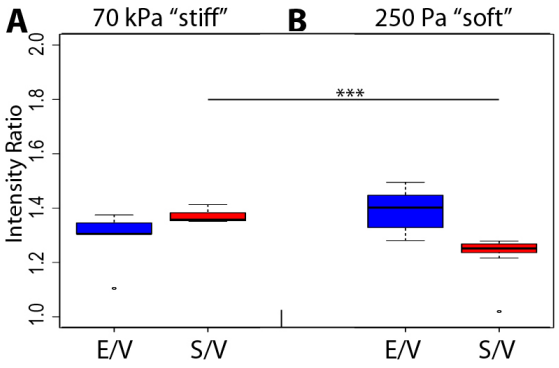

Figure 16: Side-by-side comparison of Ecad/VIN and SMAA/VIN intensity ratios for the mesenchymal region of anterior primitive streak explants on A) "stiff" (70 kPa) and B) "soft" (250 Pa) PDMS.

Next, we examine the differences between the mesenchymal region of the anterior primitive streak, which is the cell type of greatest interest in this study due to its in vivo cardiac fate. While there is no difference between the E/V on "stiff" (Figure 16a)and "soft" (Figure 16b) PDMS, the S/V ratio is significantly higher on "stiff" PDMS ($p<0.001$). We conclude that this cell type is influenced by substrate stiffness.

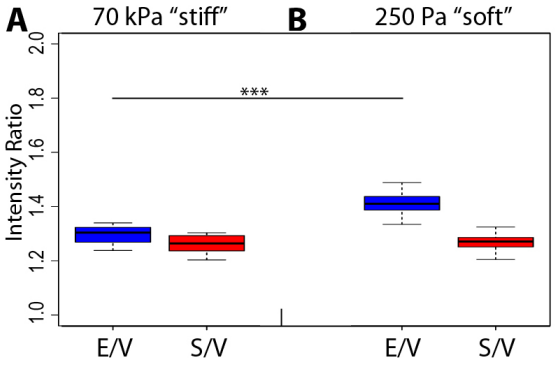

Figure 17: Side-by-side comparison of Ecad/VIN and SMAA/VIN intensity ratios for the mesenchymal posterior primitive streak explants on A) "stiff" (70 kPa) and B) "soft" (250 Pa) PDMS.

Side-by-side comparison of the posterior primitive streak explants on "soft" and "stiff" PDMS (Figure 17) revealed a statistically significant ($p<0.001$) increase in E/V on "soft" PDMS. This result suggests that the feint E-cadherin staining present at cell-cell borders in this sample group increased on the softer substrate. There was no difference in S/V values on this sample group on the two substrates.

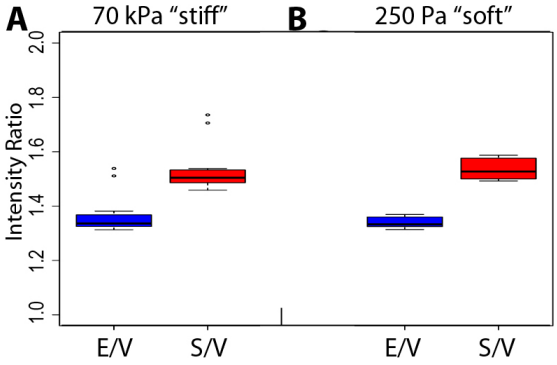

Figure 18: Side-by-side comparison of Ecad/VIN and SMAA/VIN intensity ratios for the mesenchymal cardiac cells on A) "stiff" (70 kPa) and B) "soft" (250 Pa) PDMS.

In the cardiac cell cultures on FN-coated "soft" and "stiff" PDMS, there were no statistical differences between E/V and S/V (Figure 18). This finding is significant because, although the epithelial region of the anterior primitive streak did not show differences, both the anterior and posterior primitive streak explants showed differences on "soft" and "stiff" PDMS, which suggests that cardiomyocytes from a 3-day-old quail embryo are not affected by substrate stiffness at that stage.

In summary, the most significant results in this study are as follows: 1) Anterior mesenchymal primitive streak explants (cardiac precursors) showed decreased S/V on "soft" compared to "stiff" PDMS. 2) Posterior mesenchymal primitive streak explants showed increased E/V on "soft" compared to "stiff" PDMS. 3) Cardiac cells did not show different E/V or S/V on "soft" or "stiff" PDMS. Additional findings are as follows: 4) Anterior epithelial cells have a higher E/V than other cell types on "soft"

and "stiff" PDMS, but the difference is more statistically significant on "stiff" PDMS. 5) Cardiac cells had a higher S/V than all cell types on soft and stiff.

4.4 Discussion

4.4.1 PDMS substrate selection, mechanical characterization, and ECM coating

In initial experiments, we tried using Sylgard 184 PDMS, ExCellness® substrates (a commercially-available PDMS-based polymeric material), and polyacrylamide (PA) gels to culture primitive streak explants before deciding to use Sylgard 527 PDMS, a less-common but softer silicone. Our first studies on Sylgard 184 PDMS were limited because of the lower limit of stiffness available with this material. Findings in our lab were similar to that of previous studies where the "softest" PDMS possible from this elastomer:crosslinker set is a ratio of about 55:1 with a modulus of 11kPa, [38] and that ratios of greater elastomer to crosslinker will not cure. We also cultured primitive streak explants on ExCellness® substrates. Unfortunately, the chemically-defined composition of the material was not available due to intellectual properties. Using Sylgard 184 as a high-level stiffness substrate and ExCellness® as a low-level stiffness substrate would not allow for us to control for fibronectin concentration on the substrate. Surprisingly, comparisons of cell behavior on fibronectin-coated glass, polyacrylamide gel, and Matrigel^{TM} (solubilized ECM from Engelbreth-Holm-Swarm (EHS) mouse sarcoma cells) have been made under the title of a matrix rigidity study, [54] however, different substrates adsorb different amounts of ECM proteins, and it is accepted that ECM composition and density strongly influences cell behavior. [9] Therefore, we were not comfortable using two chemically-different materials for a substrate stiffness study and moved on to manufacture PA gels. [107] Although the primitive streak explants grew on the 70 kPa FN-coated PA gels, the explants would barely attach and would not spread on the 2 kPa PA gels. We found another Sylgard PDMS formulation, Sylgard 527, that was being used in limb bud formation studies

and had tunable mechanical properties from hundreds of Pa to hundreds of kPa. [11] This was a desirable range for our study based on the stiffness of gastrula-stage embryos (around 200 Pa [44]) to fully-differentiated cardiac tissue (100+ kPa [66]). Sylgard 527 is optically clear for imaging and biologically inert, and having the same material for both soft and stiff substrates controlled for material-specific levels of fibronectin adsorption.

In this study, the 0.1:1 "stiff" PDMS and 1.5:1 "soft" PDMS required differing applications of the Hertz model to find the "true" modulus of the material as encountered by cells. The force curves (force vs. indentation depth) for "stiff" PDMS were directly fit with the Hertzian model to determine the modulus of the substrate. However, the "soft" PDMS did not have one uniform modulus regardless of indentation depth and required a point-by-point calculations of the modulus. For each indentation, the modulus (as determined by the Hertz model at each point) vs. indentation depth was plotted and the linear region was averaged to determine the modulus (Figure 9b). Many current studies looking at the role of substrate characteristics in differentiation do not fully characterize their substrates. This is problematic because false connections can be drawn between substrate stiffness and cell behavior if the substrate has been inaccurately characterized, and each lab should independently verify the substrate stiffness if it is a main variable of study. Substrate mechanics are not the same for all flexible substrates, and the models and methods used for interpreting tensile, compressive, or microindenting tests are often left unidentified in publications, [105] for example, although it has been shown that hydrogels ehibit nonlinear and viscoelastic behaviors, [95] these are rarely discussed even if experimenters mention the stress-strain curves of a hydrogel tensile test. [59] Surprisingly, *some studies present no substrate stiffness mechanical testing of any kind, even when substrate stiffness is the main variable examined in the study,* [54] [77] instead citing mechanical characterizations of formulations manufactured in other labs without

characterizing their own in-house manufacturing methods.

One interesting result in our study was the variation seen in regions throughout different preparations of the PDMS substrates (Figure 9c,d). Substrate stiffness variability is another factor not commonly identified or discussed in soft substrate cell studies. Substrates are instead commonly presented as having a uniform modulus at every scale, when we have seen that some variation at the micro-level is present in Sylgard 527 PDMS.

In addition, in studies using soft PDMS, it is not always stated what defines a "cured" substrate (as previously described, in this study a clean coverslip was sandwiched on top of our substrates, which were considered "cured" if no residue remained on the coverslip and there was no distruption to the PDMS surface after peeling off the top unattached coverslip.) For example, although our lab has previously attempted to mix 100:1 Sylgard 184 (the most commonly-used PDMS for growing cells and many related applications) and found that this ratio does not produce a fully-cured substrate even weeks after mixing, publications claim to have mixed, cured, and mechanically characterized 100:1 Sylgard 184 [105] (when other ratios such as 10:1, 30:1, 35:1, 40:1, 45:1, 50:1, and 55:1 (base/cross linker) have published Youngs moduli of 1.6 MPa and 144, 93, 48, 30, 17, and 11 kPa, respectively [38]). We find these claims suspicious, particularly curing 100:1 Sylgard 184 at 70 °C for only 24 h. Collaboration between genetics laboratories and mechanics laboratories would greatly improve current standards for substrate characterization in cell and tissue studies.

4.4.2 SMAA, ECad, and VIN image quantification distinguishes between cell types

The initial characterization of primitive streak explants and cardiac cells on glass allowed us to see that the SMAA and ECad intensities normalized to the vinculin intensity – which provided a "baseline control" for cell spreading, cell counts, and

other field-to-field morphological variation − were more accurate than the raw absolute staining intensities. Further, all ratios on glass were significantly distinct from each other ($p<0.001$ or 0.01), which suggests that our method was accurate enough to distinguish between the cell types in this study. The immunofluorescence staining without the quantification method separates the samples into only two distinct groups (Figure 19), whereas the intensity ratios capture differences between the four distinct cell types (Figure 14).

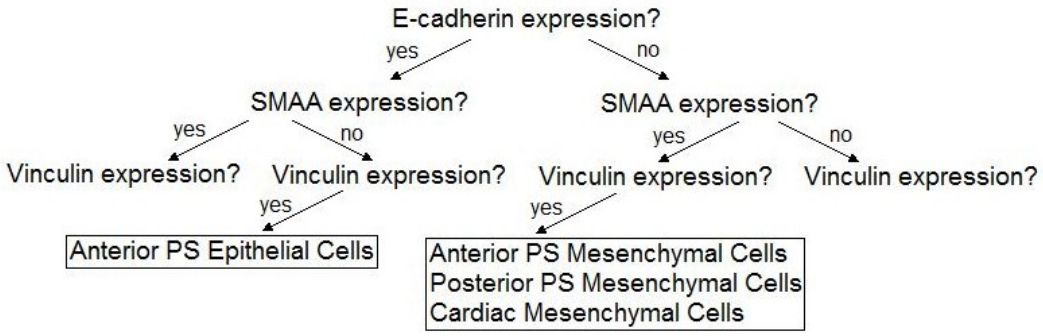

Figure 19: Decision tree representing immunofluorescence staining characterization. PS = primitive streak.

While we were pleased that the image quantification method in this study was able to determine differences in the immunofluorescence staining of four different cell types, we would like to do more localized immunoflourescence analysis in the future—akin to "localized flow cytometry" that would have the sensitivity of flow cytometry, but would not require the cells to be trypsinized and lose their spatial significance within the cultures. We would like to move to a finer "map" of staining using smaller windows within the 10 fields to display immunoflourescence staining in a more localized way.

The specific spatial differences in immunofluorescence staining that we wanted to capture in this study would not be accounted for in western blots or flow cyometry.

One of the challenges in working with embryonic cells from such a small area of the primitive streak (the location of the precardiac cells at stage HH3) is that small cell counts make it difficult to do studies that require large amounts of cells, and although we have previously completed western blots in our lab, we are uncertain that the primitive streak cell counts would be high enough for western blotting and flow cytometry. Although it is an advantage to study cardiac development in the actual precardiac cells from the embryo, the small cell counts could be a drawback that would not be present in differentiation studies using cell lines.

4.4.3 E-cadherin increases and cardiac marker SMAA decreases in presumptive cardiac cells on a softer substrate

The most important finding of this study is that the mesenchymal regions of the anterior primitive streak explants − the cells fated to become cardiac cells in vivo − have a decreased S/V on a softer PDMS substrate. Overall, comparing sample groups on "soft" and "stiff" PDMS yeilded statistical significance between different sample types on the same substrate and between the same sample type on the two different substrates stiffnesses.

4.4.3.1 E/V on "soft" and "stiff" PDMS

Comparing different sample groups on the same substrate Upon comparing the different sample types on "soft" PDMS, we found that the E/V for the epitheial anterior primitive streak was significantly higher than the other sample types ($p<0.001$) and that the E/V for the posterior primitive streak was lower than that of cardiac cells ($p<0.001$). On "stiff" PDMS, the E/V for the epitheial anterior primitive streak was still significantly higher than the other samples, but the differences were less significant than the differences on "stiff" PDMS ($p<0.05$ compared to the mesenchymal region of the anterior primitive streak and $p<0.01$ for other regions). Further, the E/V for the posterior primitive streak region on "soft" PDMS

was higher than the E/V of cardiac cells on "soft" PDMS. In light of this change in statistical significance and the fact that E/V remained the same for the epitheial anterior primitive streak explants and cardiac cells, it appears that the undifferentiated mesenchymal cells from the anterior and posterior primitive streak increased in their overall E-cadherin expression on "soft" PDMS compared to "stiff" PDMS.

Comparing the same sample groups on different substrates In addition, the posterior primitive streak cells increased their E/V on "soft" compared to "stiff" PDMS. This finding is significant because in normal ingression at the primitive streak, epithelial cells expressing E-cadherin in the epiblast shift from using E-cadherin in epithelial adherens junctions to N-cadherin in adherens junctions in the mesenchymal mesoderm cells, which is a critical change in gastrulation. [43] [12] [123] It appears that substrate stiffness effects the expression of E-cadherin in primitive streak cells, suggesting that substrate stiffness may not only play a role in cardiac differentiation, but also in other downstream phenotypes of primitive streak cells, which are not fated to form the heart. Posterior primitive streak cells do not express normally express E-cadherin in vivo. However, the substrate stiffness appears to affect their undifferentiated state. These cells are normally fated to form the intermediate mesoderm and lateral plate mesoderm, and the caudal-most end of the primitive streak contributes to the extraembryonic mesoderm, including the blood islands. [89] Substrate stiffness may be a mechanism of differentiation for these additional embryonic features.

4.4.3.2 S/V on "soft" and "stiff" PDMS

Comparing different sample groups on the same substrate Upon comparing the S/V for different sample types on "stiff" PDMS, we found that the S/V for cardiac cells was significantly higher than all other sample types ($p<0.001$) and the mesenchymal anterior primitive streak cells had a significantly higher S/V than the

posterior primitive streak ($p<0.001$). On "soft" PDMS, the S/V of cardiac cells remained higher than other cells types ($p<0.001$), but there was no statistical difference between any other cell types.

Comparing the same sample groups on different substrates When comparing the S/V of the same cell types on different substrates, there is no statistical difference in the posterior primitive streak or any cell types except for mesenchymal anterior primitive streak cells ($p<0.001$). This finding is very important because the precardiac cells reside in the anterior primitive streak at stage HH3, when explants were taken. These findings suggest that substrate stiffness has an effect on precardiac cells and may have an effect on cardiac differentiation. It is of further interest that the other cell types did *not* show statistically significant changes in SMAA expression and that cardiac cells were the only cultures that did not show any differences in marker staining on "stiff" and "soft" PDMS. It could be speculated that the 3-day-old embryonic cardiomyocytes were past a critical junction of differentiation that was exhibited in their showing the same E/V and S/V on "stiff" and "soft" PDMS.

4.4.4 Additional observations and conclusion

One interesting observation from this study was the presence of beating cultures in some of the primitive streak explants. All cardiac cultures exhibited beating. On stiff PDMS, 4 out of 12 posterior primitive streak explants were beating and 1 out of 12 anterior primitive streak explants were beating. On "soft" PDMS, 1 out of 12 posterior primitive streak explants were beating and 0 out of 12 anterior primitive streak explants were beating. This finding is initially anomalous because it is the anterior, and not the posterior, primitive streak that goes on to form the heart. However, as discussed earlier, the posterior hypoblast is one of the 2 key induction tissue interactions in cardiac development, and the hypoblast has been show to induce cardiac myocytes in anterior and posterior pre- and mid-gastrula epiblast (stage HH1,

HH3) and can induce cardiac cells in stage 4 posterior primitive streak. [114] We accordingly speculate that the culturing of the posterior primitive streak explant with some hypoblast at the base may have been more likely to beat in the presence of the hypoblast tissue.

Although our main comparison of interest in this study is on "soft" and "stiff" PDMS, the posterior primitive streak on *glass* exhibited *no epithelial regions*, whereas on 0.1:1 PDMS, it exhibited some epithelial regions and on 1.5:1 PDMS showed the most epithelial regions. When quantified, these epithelial regions of posterior primitive streak cells on PDMS were highly variable due to varying size within the 10x field (anterior primitive streak epithelial regions in this study were larger than the 10x field) and occasionally consisting of multiple cell layers that artificially increased staining levels. Therefore, we did not include the sparse epithelial regions of the posterior primitive streak in the study. Another interesting observation was the appearance of a "partial EMT" region where cells expressed SMAA but feint lines of ECad at the cell junctions were visible on some cells was seen on PDMS but not on glass. This may be why the E/V ratio on "soft" PDMS was higher than the E/V on "stiff" PDMS for the posterior primitive streak.

One of the related themes to this work in addition to cardiac differentiation is EMT because of EMT's shown dependence on substrate stiffness. [10] SMAA is the first cardiac marker, but it is has also been used as a marker of EMT. [120] Because EMT has been shown to be effected by substrate stiffness, the differentiation of cells in the streak undergoing EMT during gastrulation [72] may also be dependent on substrate stiffness. We acknowledge that there may be redundant mechanisms for upregulating SMAA in precardic cells, because these cells undergo EMT just 1 stage before transcribing SMAA. In future studies, flow cytometry and in situ hybridization may be a good next step to more fully characterize the transcription and translation of more cardiac markers in these primitive streak explants.

One advantage of this study is that we are studying the effect of substrate stiffness on cardiogenesis with isolated precardiac cells as opposed to an undifferentiated stem cell line. All necessary developmental cues up to the point of localization to the anterior primitive streak (Figure 7) have taken place, and we explant the precardiac cells 2 stages prior to the transcription of the first heart marker, SMAA. Nonetheless, we hope that the results of this study will be advantageous for ongoing studies of developing cardiac cell therapies from induced pluripotent stem cells (iPSCs) [49] and mesenchymal stem cells. [59] [78]

The heterogeneity of the primitive streak explants that necessitated our method of sample quantification was not discussed in previous cardiac cell differentiation studies on glass. We were originally struck by the heterogeneity and difficulty of finding definitive and unbiased differences between the groups. Not all regions of the same explants exhibited the same staining, and there could be variation in the stains if different fields were chosen. However, the experimenters chose the most populated and representative fields possible for each explants, and regions for each cell type were chosen carefully based on these criteria. All images were taken by the same experimenter. In addition, the experiment was repeated over a dozen times by the same experimenter, and the shown data is representative of not only the published experiment, but many additional previous experiments. Previous studies of primitive streak and early embryo explantation do not address the heterogeneity of the samples, and it is not always apparent from displayed images in previous studies.

In conclusion, here we have shown that substrate stiffness effects the behavior of anterior and posterior primitive streak cells, the former of which are fated to form the heart during embryogenesis. We hope that the results of this study will not only encourage further exploration of the effects of substrate stiffness on development and stem cell differentiation for therapeutic applications, but that cell biologists and geneticists who also study the effects of substrate stiffness will consider the importance

of mechanical characterization and collaboration with mechanicians if necessary so that results can be understood in the context of the true mechanical environment, specifically, substrate stiffness in vivo.

Chapter V

FUTURE CONSIDERATIONS

We have shown in these studies that the primitive streak stiffens relative to the pre-primitive streak embryo and that regions outside the primitive streak soften over time. Our explantation studies show that precardiac primitive streak cells are sensitive to substrate stiffness. In other words, these primitive streak cells respond to changes in the stiffness, which are occurring in the gastrula-stage embryo. Tissue stiffness and substrate stiffness are not independent. The interplay between these variables is relevant to the study of the mechanical environment because the tissue stiffness is changing and the cells are sensitive to changes in substrate stiffness.

At the gastrula stage, the embryo is only attached to external tissue (specifically, the vitelline membrane) at the outer edges. The embryo as a whole (comprised of the three germ layers) is in tension and anchored by the vitelline membrane around the periphery. The increased tension in the embryo would increase the apparent stiffness, much like a stretched lab glove appears to be more stiff when stretched. (Our explants were removed from the embryo to avoid this apparent increase in stiffness in our AFM experiments.) However, the tension not only changes the apparent stiffness of the tissue, it can alter the apparent stiffness of the ECM. The ECM does not actively contract, but it does have a passive response to tension and compression. Beneath the epiblast layer is a thin ECM layer termed the basement membrane comprised of fibronectin, laminin, collagen I and collagen IV. Fibronectin is an elastic protein structure that can unfold under tension, presenting additional cell-binding motifs. In addition, the contraction of cells, such as at the primitive streak, could conversely contract the ECM around them, thus hiding cell-binding motifs. The density of

the ECM can affect its stiffness as well, and future studies on the changing ECM modeling by primitive streak cells would benefit understanding of the role of ECM in gastrulation.

In this study, we have shown the importance of the mechanical microenvironment in the developmental processes of gastrulation and cardiac specification. In the field of gastrulation, apical constriction has long been an accepted mechanism for anamniotes and lower orders, and we hope that this critical mechanism becomes universally accepted in amniote gastrulation. There are many other developmental processes that display a feat of biophysical control, such as neural tube closure, heart looping and septation, and dorsal elongation (the mechanics of which are currently studied in *Xenopus laevis* in the Davidson Lab [121]), which would benefit from further study as to how the genome codes for these extreme mechanical changes. Though some classical and modern approaches have been used to measure the forces generated and mechanical changes in the embryo, developmental studies by and large approach morphogensis from a purely genetic standpoint. We hope that this study encourages a greater appreciation and study of the mechanical environment during embryogenesis.

One weakness in the study of rho-kinase (ROCK)-activated actomyosin contractility is the multiple effects of of the small-molecule inhibitor Y-27632. By inhibiting ROCK with Y-27632, we could potentially be desurbing several signaling pathways in which ROCK is involved including cell adhesion and proliferation. In addition, in the study of cell convergence to the primitive streak using time−lapse microscopy, we used Y-27632 on the whole embryo, whereas ideally given our hypothesis that actomyosin contractility at the primitive streak "pulls" the cell sheets in the epiblast towards itself, we would be able to inhibit actomyosin contractility *locally* at the primitive streak before observing changes in cell velocity towards the primitive streak. This may be accomplished with electroporation of an actomyosin contractility inhibitor at a pre-primitive streak stage, but controlling the timing of translation and

localization of such an inhibitor would be challenging. Another method may be a localized administration of a drug treatment, however, containment of the drug may be an issue.

The importance of the effect of mechanical cues—and specifically substrate stiffness—on differentiation during development and directed stem cell differentiation has become generally accepted over the past decade. However, there is sometimes a lack of mechanical characterization of substrates in published studies that specifically focus on the role of substrate stiffness in differentiation. While genetic studies are important in this area, and some labs may excel in genetic analysis, the results of their studies cannot be trusted if there is no mechanical characterization of the variable substrate stiffness. In addition, it is important to recognize when conducting studies of the effects of substrate stiffness that ECM protein composition as well as density must be the same on substrates of varying stiffnesses of that only one variable at a time is modified.

In future studies continuing to look at the effect of substrate stiffness on cardiac differentiation, additional characterization methods such as in situ hybridization and flow cytometry may provide valuable additional insights, even though spatial differences would not be measureable with flow cytometry, overall levels of cardiac markers undetectable with immonofluorescence staining such as $\alpha-$actinin and N-cadherin may be present and visible in a flow cytometry study. The only challenge for flow cytometry studies on embryonic explants is the cell counts of the samples. Many samples ($\sim$25 explants minimum) would have to be combined, which may dilute the differences between embryos in the same sample groups. SMAA is originally transcripted and stage HH 5 but not translated until HH 9. One phenomena not explored in this study is the transcription of SMAA—our immunoflourescence staining reveals only translated SMAA proteins. Also, we believe that some of the smaller markers that we tried to see with immunofluoresence stainging, such as transcription factor

Nkx2.5, may only be visible with in situ hybridization analysis or flow cytometry. Not only would in situ hybridization allow for SMAA *transcription* characterization in addition to the translated SMAA characterization seen in immunofluorescence studies, but also other markers that may not have translational modulation but show transcriptional modulation could be detected.

A definite goal for future studies should be to exploit the range of Sylgard 527 PDMS and include more substrate stiffness groups between 250 Pa and 70 kPa to see what is the "threshold" for the differences in SMAA, E-cadherin, and vinculin staining shown in this study.

In this study, we found that anterior and posterior primitive streak cells were sensitive to substrate stiffness, but 3-day-old cardiomyocytes were not. We could go on to speculate that the cardiac cells have already passed a junction of differentiation based on substrate stiffness and that the precardiac cells we cultured were not past this specification point. However, we could take precardiac cells from earlier and later stages than from the anterior primitive streak at stage HH 3. Further work could look at not only taking cells from stage 1 Kollers sickle, but the heart forming regions (HFRs) as well. Another additional study of interest would be to add combinations of the array of signaling molecules during precardic cell interaction with the posterior hypoblast at stage 1 and with interaction with the anterior lateral endoderm at stage HH 5. The field would benefit from studies that examined not just the substrate stiffness or combination of signaling molecules, but the *interaction* between these two variables.

It is interesting not only that precardiac cells in the anterior primitive streak were influenced by substrate stiffness, but that the posterior primitive streak cells were also influenced as well. This suggests that other developmental processes may depend on a desired range of ECM stiffness, and we hope that experimenters in the fields of developmental biology and stem cell differentiation will continue to look at the role

of substrate stiffness in differentiation.

REFERENCES

[1] Ubirajara Agero, James A Glazier, and Michael Hosek. Bulk elastic properties of chicken embryos during somitogenesis. *Biomed Eng Online*, 9:1–16, 2010.

[2] J. Alcaraz, R. Xu, H. Mori, C. M. Nelson, R. Mroue, V. A. Spencer, D. Brownfield, D. C. Radisky, C. Bustamante, and M. J. Bissell. Laminin and biomimetic extracellular elasticity enhance functional differentiation in mammary epithelia. *EMBO Journal*, 27(21):2829–38–, 2008.

[3] P.D. Allison. Missing Data. Sage Publications, Inc., Thousand Oaks, California, 2002. pp. 27-36.

[4] José Luis Alonso and Wolfgang H Goldmann. Feeling the forces: atomic force microscopy in cell biology. *Life Sciences*, 72(23):2553–2560, April 2003.

[5] Steven S An, Rachel E Laudadio, Jean Lai, Rick A Rogers, and Jeffrey J Fredberg. Stiffness changes in cultured airway smooth muscle cells. *American journal of physiology. Cell physiology*, 283(3):C792–801, September 2002.

[6] P. B. Antin, R. G. Taylor, and T. Yatskievych. Precardiac mesoderm is specified during gastrulation in quail. *Dev Dyn*, 200(2):144–54–, 1994.

[7] P. B. Antin, T. Yatskievych, J. L. Dominguez, and P. Chieffi. Regulation of avian precardiac mesoderm development by insulin and insulin-like growth factors. *J Cell Biol*, 168(1):42–50–, 1996.

[8] G Bao and S Suresh. Cell and molecular mechanics of biological materials. *Nature materials*, 2(11):715–25, November 2003.

[9] TH Barker. The role of ecm proteins and protein fragments in guiding cell behavior in regenerative medicine. *Biomaterials*, 32(18):4211–4. doi: 10.1016/j.biomaterials.2011.02.027., 2011.

[10] AC Brown, VF Fiore, TA Sulchek, and TH Barker. Physical and chemical microenvironmental cues orthogonally control the degree and duration of fibrosis-associated epithelial to mesenchymal transition. *J Pathol*, 229(1):25–35, 2012.

[11] S. Calve and Simon H.G. Extracellular control of limb regeneration. *IUTAM Bookseries*, 16:257–266, 2010.

[12] A Cano, MA Pérez-Moreno, I Rodrigo, A Locascio, MJ Blanco, MG del Barrio, F Portillo, and MA Nieto. The transcription factor snail controls epithelial-mesenchymal transitions by repressing e-cadherin expression. *Nat Cell Biol*, 2(2):76–83, 2000.

[13] S. C. Chapman, J. Collignon, G. C. Schoenwolf, and A. Lumsden. Improved method for chick whole-embryo culture using a filter paper carrier. *Dev Dyn*, 220(3):284–289, 2001.

[14] C. Cheng, R. Stewardjr, and P. Leduc. Probing cell structure by controlling the mechanical environment with cellsubstrate interactions. *J Biomech*, 42(2):187–192, 2009.

[15] Manli Chuai and Cornelis J Weijer. The mechanisms underlying primitive streak formation in the chchick embryo. *Curr Top Dev Biol*, 81(2):135–56, January 2008.

[16] Manli Chuai and Cornelis J Weijer. Who moves whom during primitive streak formation in the chick embryo. *HFSP journal*, 3(2):71–6, January 2009.

[17] Manli Chuai and Cornelis Jan Weijer. Regulation of cell migration during chick gastrulation. *Current opinion in genetics & development*, 19(4):343–9, August 2009.

[18] Manli Chuai, Wei Zeng, Xuesong Yang, Veronika Boychenko, James a Glazier, and Cornelis J Weijer. Cell movement during chick primitive streak formation. *Developmental biology*, 296(1):137–49, August 2006.

[19] J. F. Colas, A. Lawson, and G. C. Schoenwolf. Evidence that translation of smooth muscle alpha-actin mrna is delayed in the chick promyocardium until fusion of the bilateral heart-forming regions. *Dev Dyn*, 218(2):316–30, 2000.

[20] Vito Conte, José J Muñoz, Buzz Baum, and Mark Miodownik. Robust mechanisms of ventral furrow invagination require the combination of cellular shape changes. *Physical biology*, 6(1):016010, January 2009.

[21] A Czirók, P A Rupp, B J Rongish, and C D Little. Multi-field 3D scanning light microscopy of early embryogenesis. *Journal of microscopy*, 206(Pt 3):209–17, June 2002.

[22] L A Davidson, G F Oster, R E Keller, and M A R Koehl. Measurements of mechanical properties of the blastula wall reveal which hypothesized mechanisms of primary invagination are physically plausible in the sea urchin Strongylocentrotus purpuratus. *Dev Biol*, 209. part 2(1999):221–238, 1999.

[23] Lance A. Davidson, M. A. R. Koehl, Raymond Keller, and George F. Oster. How do sea urchins invaginate? using biomechanics to distinguish between mechanisms of primary invagination. *Development*, 121:2005–2018, 1995.

[24] J. P. de Winter, P. ten Dijke, C. J. de Vries, T. A. van Achterberg, H. Sugino, P. de Waele, D. Huylebroeck, K. Verschueren, and A. J. van den Eijnden-van Raaij. Follistatins neutralize activin bioactivity by inhibition of activin binding to its type ii receptors. *Mol Cell Endocrinol*, 116(1):105–14, 1996.

[25] R. L. Dehaan. Migration patterns of the precardiac mesoderm in the early chick embrvo. *Exp Cell Res*, 29:544–60, 1963.

[26] Mitchell DeJonge, David Burchfield, Barry Bloom, Maria Duenas, Whit Walker, Mark Polak, Elizabeth Jung, Dietra Millard, Robert Schelonka, Fabien Eyal, Amy Morris, Barry Kapik, Destrey Roberson, Karen Kesler, Joe Patti, and Seth Hetherington. Clinical Trial of Safety and Efficacy of IHN-A21 for the Prevention of nosocomial staphylococcal bloodstream infection in premature infants. *J Pediatr.*, 151:260–265, 2007.

[27] M. C. DeRuiter, R. E. Poelmann, M. M. Mentink, L. Vaniperen, and A. C. Gittenberger-De Groot. Early formation of the vascular system in quail embryos. *Anat Rec*, 235(2):261–74, 1993.

[28] D. E. Discher, P. Janmey, and Y. L. Wang. Tissue cells feel and respond to the stiffness of their substrate. *Science*, 310(5751):1139–1143, 2005.

[29] A Rogier T Donders, Geert J M G van der Heijden, Theo Stijnen, and Karel G M Moons. Review: a gentle introduction to imputation of missing values. *Journal of clinical epidemiology*, 59(10):1087–91, October 2006.

[30] L. M. Eisenberg and C. A. Eisenberg. An in vitro analysis of myocardial potential indicates that phenotypic plasticity is an innate property of early embryonic tissue. *Stem Cells and Development*, 13(6):614–24, 2004.

[31] A. J. Engler, C. Carag-Krieger, C. P. Johnson, M. Raab, H. Y. Tang, D. W. Speicher, J. W. Sanger, J. M. Sanger, and D. E. Discher. Embryonic cardiomyocytes beat best on a matrix with heart-like elasticity: scar-like rigidity inhibits beating. *Journal of Cell Science*, 121(22):3794–3802, 2008.

[32] A. J. Engler, S. Sen, H. L. Sweeney, and D. E. Discher. Matrix elasticity directs stem cell lineage specification. *Journal of Cell Science*, 126(4):677–89, 2006.

[33] H Eyal-Giladi and S Kochav. From cleavage to primitive streak formation: a complementary normal table and a new look at the first stages of the development of the chick. I. General morphology. *Developmental biology*, 49(2):321–37, April 1976.

[34] M. Gannon and D. Bader. Initiation of cardiac differentiation occurs in the absence of anterior endoderm. *Development*, 121(8):2439–50, 1995.

[35] V. Garcia-Martinez and G. C. Schoenwolf. Primitive-streak origin of the cardiovascular system in avian embryos. *Dev Biol*, 159(2):706–19, 1993.

[36] SF Gilbert. *Developmental Biology. 6th edition.* Sunderland (MA): Sinauer Associates, 2000.

[37] A. Gonzalez-Sanchez and D. Bader. In vitro analysis of cardiac progenitor cell differentiation. *Dev Biol*, 139(1):197–209, 1990.

[38] Ovidiu D. Gordan, Bo N. J. Persson, Claudia M. Cesa, Dirk Mayer, Bernd Hoffmann, Sabine Dieluweit, and Rudolf Merkel. On pattern transfer in replica molding. *Langmuir*, 24:6636–6639, 2008.

[39] W. H. Guo, M. T. Frey, N. A. Burnham, and Y. L. Wang. Substrate rigidity regulates the formation and maintenance of tissues. *Biophys J*, 90(6):2213–20, 2006.

[40] Viktor Hamburger and Howard L Hamilton. A series of normal stages in the development of the chick embryo. *J Morphol*, 88(1):49–92, 1951.

[41] J Hardin and R Keller. The behaviour and function of bottle cells during gastrulation of Xenopus laevis. *Development (Cambridge, England)*, 103(1):211–30, May 1988.

[42] Y. Hatada and C. D. Stern. A fate map of the epiblast of the early chick embryo. *Development*, 120(10):2879–89, 1994.

[43] K Hatta and M Takeichi. Expression of n-cadherin adhesion molecules associated with early morphogenetic events in chick development. *Nature*, 320(6061):447–9, 1986.

[44] J Henkels, J Oh, W Xu, D Owen, T Sulchek, and E Zamir. Spatiotemporal mechanical variation reveals critical role for rho kinase during primitive streak morphogenesis. *Ann Biomed Eng*, 41(2):421–32, 2013.

[45] T. Inagaki, V. Garcia-Martinez, and G. C. Schoenwolf. Regulative ability of the prospective cardiogenic and vasculogenic areas of the primitive streak during avian gastrulation. *Dev Dyn*, 197(1):57–68, 1993.

[46] B. C. Isenberg, P. A. DiMilla, M. Walker, S. Kim, and J. Y. Wong. Vascular smooth muscle cell durotaxis depends on substrate stiffness gradient strength. *Biophysical Journal*, 97(5):1313–1322, 2009.

[47] K L Johnson. *Contact Mechanics*. Cambridge University Press, 1985.

[48] K L Johnson, K Kendall, and A D Roberts. Surface energy and the contact of elastic solids. *Proceedings of the Royal Society of London*, 324:301–313, 1971.

[49] Tsukasa Kamakura, Takeru Makiyama, Kenichi Sasaki, Yoshinori Yoshida, Yimin Wuriyanghai, Jiarong Chen, Tetsuhisa Hattori, Seiko Ohno, Toru Kita, Minoru Horie, ShinyaMD Yamanaka, and Takeshi Kimura. Ultrastructural maturation of human-induced pluripotent stem cell-derived cardiomyocytes in a long-term culture. *Circulation Journal*, (doi: 10.1253/circj.CJ-12-0987), 2013.

[50] Ray Keller, Lance A. Davidson, and David R. Shook. How we are shaped: The biomechanics of gastrulation. *Differentiation*, 71:171–205, 2003.

[51] Elizabeth Laxson Kimberly and Jeff Hardin. Bottle cells are required for the initiation of primary invagination in the sea urchin embryo. *DEVELOPMENTAL BIOLOGY*, 204:235–250, 1998.

[52] Margaret L. Kirby. *Cardiac Development*. Oxford University Press, 2007.

[53] M. Krieg, Y. Arboleda-Estudillo, P. H. Puech, J. Kfer, F. Graner, D. J. Mller, and C. P. Heisenberg. Tensile forces govern germ-layer organization in zebrafish. *Nature Cell Biology*, 10(4):429–436, 2008.

[54] Kshitiz, Maimon E. Hubbi, Eun Hyun Ahn, John Downey, Junaid Afzal, Deok-Ho Kim, Sergio Rey, Connie Chang, Arnab Kundu, Gregg L. Semenza, Roselle M. Abraham, and Andre Levchenko. Matrix rigidity controls endothelial differentiation and morphogenesis of cardiac precursors. *Sci. Signal.*, 5(227):p. ra41 DOI: 10.1126/scisignal.2003002, 2012.

[55] A. N. Ladd, T. A. Yatskievych, and P. B. Antin. Regulation of avian cardiac myogenesis by activin/tgfbeta and bone morphogenetic proteins. *Dev Biol*, 204(2):407–19, 1998.

[56] NM. LeDouarin. Particularites du noyau interphasique chez la caille japonaise (coturnix coturnix japonica): utilisation de ces particularites "marquage biologique" dans les recherches sur les interactions tissulaires et le migration cellulaire en cours de l'ontogenese. *Bull Biol Fr Belg*, 103:435–452, 1969.

[57] Jen-Yi Lee and Richard M Harland. Actomyosin contractility and microtubules drive apical constriction in Xenopus bottle cells. *Developmental biology*, 311(1):40–52, November 2007.

[58] M. Li, T. Cui, D. K. Mills, Y. M. Lvov, and M. J. McShane. Comparison of selective attachment and growth of smooth muscle cells on gelatin- and fibronectin-coated micropatterns. *Journal of Nanoscience and Nanotechnology*, 5(11):1809–1815, 2005.

[59] Z Li, X Guo, AF Palmer, H Das, and J Guan. High-efficiency matrix modulus-induced cardiac differentiation of human mesenchymal stem cells inside a thermosensitive hydrogel. *Acta Biomater.*, 8(10):3586–95 doi: 10.1016/j.actbio.2012.06.024. Epub 2012 Jun 21., 2012.

[60] K. K. Linask. N-cadherin localization in early heart development and polar expression of na+,k(+)-atpase, and integrin during pericardial coelom formation and epithelialization of the differentiating myocardium. *Dev Biol*, 151(1):213–24, 1992.

[61] C. M. Lo, H. B. Wang, M. Dembo, and Y. L. Wang. Cell movement is guided by the rigidity of the substrate. *Biophys J*, 79(1):144–52, 2000.

[62] J. Lough, M. Barron, M. Brogley, Y. Sugi, D. L. Bolender, and X. Zhu. Combined bmp-2 and fgf-4, but neither factor alone, induces cardiogenesis in non-precardiac embryonic mesoderm. *Dev Biol*, 178(1):198–202, 1996.

[63] Jose R Lozano, Daniel Kiracofe, John Melcher, Ricardo Garcia, and Arvind Raman. Calibration of higher eigenmode spring constants of atomic force microscope cantilevers. *Nanotechnology*, 21(46):465502 (7pp), November 2010.

[64] Craig R. Magie, Marymegan Daly, and Mark Q. Martindale. Gastrulation in the cnidarian nematostella vectensis occurs via invagination not ingression. *Developmental Biology*, 305:483497, 2007.

[65] Adam C. Martin, Matthias Kaschube, and Eric F. Wieschaus. Pulsed contractions of an actinmyosin network drive apical constriction. *Nature*, doi:10.1038/nature07522, 2008.

[66] Anshu B. Mathura, Amy M. Collinswortha, William M. Reicherta, William E. Krausb, and George A. Truskeya. Endothelial, cardiac muscle and skeletal muscle exhibit different viscous and elastic properties as determined by atomic force microscopy. *Journal of Biomechanics*, 34(12):15451553, 2001.

[67] H. Matsui, M. Sakabe, H. Sakata, N. Yanagawa, K. Ikeda, T. Yamagishi, and Y. Nakajima. Induction of initial heart alpha-actin, smooth muscle alpha-actin, in chick pregastrula epiblast: the role of hypoblast and fibroblast growth factor-8. *Development, Growth, and Differentiation*, 50(3):143–57, 2008.

[68] Hiroko Matsui, Kazuo Ikeda, Kazuki Nakatani, Masahide Sakabe, Toshiyuki Yamagishi, Toshio Nakanishi, and Yuji Nakajima. Induction of initial cardiomyocyte -actinsmooth muscle -actinin cultured avian pregastrula epiblast: A role for nodal and bmp antagonist. *Dev Dyn*, 233(4):1419–1429, 2005.

[69] E. Mitrani, T. Ziv, G. Thomsen, Y. Shimoni, D. A. Melton, and A. Bril. Activin can induce the formation of axial structures and is expressed in the hypoblast of the chick. *Cell*, 63(3):495–501, 1990.

[70] S W Moore, R E Keller, and M a Koehl. The dorsal involuting marginal zone stiffens anisotropically during its convergent extension in the gastrula of Xenopus laevis. *Development (Cambridge, England)*, 121(10):3131–40, October 1995.

[71] R. A. Moreno-Rodriguez, E. L. Krug, L. Reyes, L. Villavicencio, C. H. Mjaatvedt, and R. R. Markwald. Bidirectional fusion of the heart-forming fields in the developing chick embryo. *Dev Dyn*, 235(1):191–202, 2006.

[72] Yukiko Nakaya and Guojun Sheng. Epithelial to mesenchymal transition during gastrulation—an embryological view. *Develop. Growth Differ.*, 50:755766. doi: 10.1111/j. 1440–169X.2008.01070.x, 2008.

[73] Yukiko Nakaya, Erike W Sukowati, Yuping Wu, and Guojun Sheng. RhoA and microtubule dynamics control cell-basement membrane interaction in EMT during gastrulation. *Nature cell biology*, 10(7):765–75, July 2008.

[74] D A T New. A new technique for the cultivation of the chick embryo in vitro. *J. Embryol. exp. Morph.*, 3. part 4:320–31, 1955.

[75] F. Orts Llorca. Influence of the endoblast in the morphogenesis and late differentiation of the chick heart. *Acta Anat (Basel)*, 52:202–14, 1963.

[76] E. A. Osborn, A. Rabodzey, Jr. Dewey, C. F., and J. H. Hartwig. Endothelial actin cytoskeleton remodeling during mechanostimulation with fluid shear stress. *Physiol Cell Physiol*, 290(2):C444–52, 2006.

[77] J Park, HN Kim, DH Kim, A Levchenko, and KY Suh. Quantitative analysis of the combined effect of substrate rigidity and topographic guidance on cell morphology. *IEEE Trans Nanobioscience*, 11(1):28–36. doi: 10.1109/TNB.2011.2165728., 2012.

[78] Mark F. Pittenger and Bradley J. Martin. Mesenchymal stem cells and their potential as cardiac therapeutics. *Circ Res.*, 95:9–20, 2004.

[79] R E Poelmann, A C Gittenberger-de Groot, M M Mentink, Bkenkamp R, and B Hogers. Development of the cardiac coronary vascular endothelium, studied with antiendothelial antibodies, in chicken-quail chimeras. *Circulation Research*, 73:559–568, 1993.

[80] M Radmacher. Measuring the elastic properties of biological samples with the afm. *IEEE Eng Med Biol Mag.*, 16:47–57, 1997.

[81] M. E. Rawles. The heart-forming areas of the early chick blastoderm. *Physiol Zool*, 16:22–42, 1943.

[82] C. A. Reinhart-King, M. Dembo, and D. A. Hammer. Cell-cell mechanical communication through compliant substrates. *Biophys J*, 95(12):6044–6051, 2008.

[83] Domenico Ribatti. William harvey and the discovery of the circulation of the blood. *J Angiogenes Res*, 1:3, 2009.

[84] PA Rupp, BJ Rongish, A Czirok, and CD Little. Culturing of avian embryos for time-lapse imaging. *Biotechniques*, 32:274–8, 2003.

[85] D. L. Ruzicka and R. J. Schwartz. Sequential activation of alpha-actin genes during avian cardiogenesis: vascular smooth muscle alpha-actin gene transcripts mark the onset of cardiomyocyte differentiation. *Journal of Cell Biology*, 107(6 Pt 2):2575–86, 1988.

[86] A. Saez, M. Ghibaudo, A. Buguin, P. Silberzan, and B. Ladoux. Rigidity-driven growth and migration of epithelial cells on microstructured anisotropic substrates. *Proc Natl Acad Sci USA*, 104(20):8281–6, 2007.

[87] S A Sandersius, M Chuai, C J Weijer, and T J Newman. A 'chemotactic dipole' mechanism for large-scale vortex motion during primitive streak formation in the chick embryo. *Physical biology*, 8(4):045008, August 2011.

[88] Jacob M. Sawyer, Jessica R. Harrell, Gidi Shemer, Jessica Sullivan-Brown, Minna Roh-Johnson, and Bob Goldstein. Apical constriction: A cell shape change that can drive morphogenesis. *Developmental Biology*, 341:5–19, 2010.

[89] GC Schoenwolf, V Garcia-Martinez, and MS Dias. Mesoderm movement and fate during avian gastrulation and neurulation. *Dev Dyn*, 193(3):235–48, 1992.

[90] T. M. Schultheiss, S. Xydas, and A. B. Lassar. Induction of avian cardiac myogenesis by anterior endoderm. *Development*, 121(12):4203–14, 1995.

[91] Thomas M. Schultheiss, J. B. Burch, and A. B. Lassar. A role for bone morphogenic proteins in the induction of cardiac myogenesis. *Genes & Development*, 8:451 – 462, 1997.

[92] M. A. Selleck and C. D. Stern. Fate mapping and cell lineage analysis of hensen's node in the chick embryo. *Development*, 112(2):615–26, 1991.

[93] JM Slack. *From egg to embryo. Determinative events in early development.* Cambridge University Press, 1983.

[94] H. Stalsberg and R. L. DeHaan. The precardiac areas and formation of the tubular heart in the chick embryo. *Dev Biol*, 19(2):128–59, 1969.

[95] Jason A. Stammen, Stephen Williams, David N. Ku, and Robert E. Guldberg. Mechanical properties of a novel pva hydrogel in shear and unconfined compression. *Biomaterials*, 22:799–806, 2001.

[96] C. D. Stern and D. R. Canning. Gastrulation in birds: a model system for the study of animal morphogenesis. *Experientia*, 44:651–7, 1988.

[97] C. D. Stern, R. T. Yu, A. Kakizuka, C. R. Kintner, L. S. Mathews, W. W. Vale, R. M. Evans, and K. Umesono. Activin and its receptors during gastrulation and the later phases of mesoderm development in the chick embryo. *Dev Biol*, 172(1):192–205, 1995.

[98] Y. Sugi and J. Lough. Onset of expression and regional deposition of alpha-smooth and sarcomeric actin during avian heart development. *Dev Dyn*, 193(2):116–24, 1992.

[99] Y. Sugi and J. Lough. Activin-a and fgf-2 mimic the inductive effects of anterior endoderm on terminal cardiac myogenesis in vitro. *Dev Biol*, 168(2):567–74, 1995.

[100] Y Sugi, J Sasse, and J Lough. Inhibition of precardiac mesoderm cell proliferation by antisense oligodeoxynucleotide complementary to fibroblast growth factor-2 (fgf-2). *Dev Biol*, 157(1):28–37, 1993.

[101] L. A. Taber and S. Chabert. Theoretical and experimental study of growth and remodeling in the developing heart. *Biomechanics and Modeling in Mechanobiology*, 1(1):29–43, 2002.

[102] L. A. Taber, N. Hu, T. Pexieder, E. B. Clark, and B. B. Keller. Residual strain in the ventricle of the stage 16-24 chick embryo. *Circ Res*, 72(2):455–62, 1993.

[103] S. Takeuchi. Wound healing in the cornea of the chick embryo. iv. promotion of the migratory activity of isolated corneal epithelium in culture by the application of tension. *Dev Biol*, 70(1):232–40, 1979.

[104] Carlos Tamulonis, Marten Postma, Heather Q. Marlow, Craig R. Magie, Johann de Jong, and Jaap Kaandorp. A cell-based model of nematostella vectensis gastrulation including bottle cell formation, invagination and zippering. *Developmental Biology*, 351:217–228, 2011.

[105] B Trappmann, JE Gautrot, JT Connelly, DG Strange, Y Li, ML Oyen, MA Cohen Stuart, H Boehm, B Li, V Vogel, JP Spatz, FM Watt, and WT Huck. Extracellular-matrix tethering regulates stem-cell fate. *Nat Mater*, 11(7):642–9, 2012.

[106] John Philip Trinkaus. *Cells into Organs: The Forces That Shape the Embryo*. Prentice-Hall, 1984.

[107] Justin R. Tse and Adam J. Engler. Preparation of hydrogel substrates with tunable mechanical properties. *Current Protocols in Cell Biology*, (DOI: 10.1002/0471143030.cb1016s47), 2010.

[108] L. Vakaet. Some new data concerning the formation of the definitive endoblast in the chick embryo. *J Embyol Exp Morphol*, 10:38–57, 1962.

[109] Bakhtier Vasiev, Ariel Balter, Mark Chaplain, James A. Glazier, and Cornelis J. Weijer. Modeling gastrulation in the chick embryo: Formation of the primitive streak. *PLoS ONE*, 5 (5):e10571, 2010.

[110] Octavian Voiculescu, Federica Bertocchini, Lewis Wolpert, Ray E Keller, and Claudio D Stern. The amniote primitive streak is defined by epithelial cell intercalation before gastrulation. *Nature*, 449(7165):1049–52, October 2007.

[111] N Wang, IM Toli-Nrrelykke, J Chen, SM Mijailovich, JP Butler, JJ Fredberg, and D Stamenovi. Cell prestress. i. stiffness and prestress are closely associated in adherent contractile cells. *Am J Physiol Cell Physiol*, 282. part 3:C606–16, 2002.

[112] L Wei, K Imanaka-Yoshida, L Wang, S Zhan, MD Schneider, FJ DeMayo, and RJ Schwartz. Inhibition of rho family gtpases by rho gdp dissociation inhibitor disrupts cardiac morphogenesis and inhibits cardiomyocyte proliferation. *Development*, 129. part 7:1705–14, 2002.

[113] Wenwei Xu, Nadeen Chahine, and Todd Sulchek. Extreme hardening of PDMS thin films due to high compressive strain and confined thickness. *Langmuir : the ACS journal of surfaces and colloids*, 27(13):8470–7, July 2011.

[114] T. A. Yatskievych, A. N. Ladd, and P. B. Antin. Induction of cardiac myogenesis in avian pregastrula epiblast: the role of the hypoblast and activin. *Development*, 124(13):2561–70–, 1997.

[115] JL Young and AJ Engler. Hydrogels with time-dependent material properties enhance cardiomyocyte differentiation in vitro. *Biomaterials*, 32(4):1002–9, 2011.

[116] EA Zamir, V Srinivasan, R Perucchio, and LA Taber. Mechanical asymmetry in the embryonic chick heart during looping. *Ann Biomed Eng*, 31. part 11:1327–36, 2003.

[117] EA Zamir and LA Taber. On the effects of residual stress in microindentation tests of soft tissue structures. *J Biomech Eng*, 126. part 2:276–83, 2004.

[118] Evan A Zamir, Brenda J Rongish, and Charles D Little. The ECM moves during primitive streak formation–computation of ECM versus cellular motion. *PLoS biology*, 6(10):e247, October 2008.

[119] Evan A Zamir and Larry A Taber. Material Properties and Residual Stress in the Stage 12 Chick Heart During Cardiac Looping. *Journal of Biomechanical Engineering*, 126(6):823, 2004.

[120] M Zeisberg and EG Neilson. Biomarkers for epithelial-mesenchymal transitions. *J Clin Invest*, 119(6):1429–37. doi: 10.1172/JCI36183, 2009.

[121] J. Zhou, H. Y. Kim, and L. A. Davidson. Actomyosin stiffens the vertebrate embryo during critical stages of elongation and neural tube closure. *Development*, 136:677–688, 2009.

[122] Jian Zhou, Hye Young Kim, and Lance A Davidson. Actomyosin stiffens the vertebrate embryo during crucial stages of elongation and neural tube closure. *Development (Cambridge, England)*, 136(4):677–88, February 2009.

[123] IE Zohn, Y Li, EY Skolnik, KV Anderson, J Han, and L Niswander. p38 and a p38-interacting protein are critical for downregulation of e-cadherin during mouse gastrulation. *Cell*, 125(5):957–69, 2006.

VITA

Julia Ann Henkels attended St. Thomas More School and Bethel Park High School in Bethel Park, Pennsylvania. In 2006, she completed a Bachelor of Science in Mechanical Engineering at the University of Notre Dame and in 2007 completed a Master of Science in Mechanical Engineering. In 2008 she began her doctoral work in Bioengineering at Georgia Institute of Technology.

Experiments, 1996

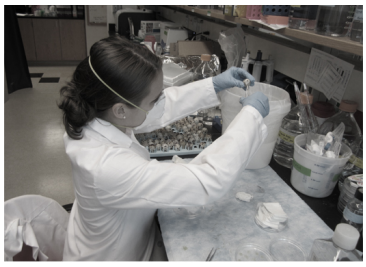

Experiments, 2012